Title: **A Dapl1+ subpopulation of naïve CD8 T cells contains committed precursors of memory lineage.**

Authors: Adam Lynch (first author), Kaito A. Hioki, Xueting Liang, Iris Thesmar, Julia Cernjul, Xinjian He, Jesse Mager, Wei Cui, Dominique Alfandari, Elena L. Pobezinskaya (last author), Leonid A. Pobezinsky (last author).

Key words: stem-like, memory CD8 T cells, differentiation, thymus, let-7, Lin28b, neonatal, T regulatory cells, CD62L, Tim-3

Affiliations + emails

Adam Lynch:

Aclynch@umass.edu

Animal Biotechnology and Biomedical Sciences Program, University of Massachusetts, Amherst, MA, USA

Department of Veterinary and Animal Science, University of Massachusetts, Amherst, MA, USA

UMass Biotech Training Program (BTP), Amherst, MA, USA

Kaito A. Hioki:

Khioki@umass.edu

Molecular and Cellular Biology Program, University of Massachusetts, Amherst MA, USADepartment of Veterinary and Animal Science, University of Massachusetts, Amherst, MA, USA

UMass Biotech Training Program (BTP), Amherst, MA, USA

Xueting Liang:

Xuetingliang@umass.edu

Animal Biotechnology and Biomedical Sciences Program, University of Massachusetts, Amherst, MA, USA
Department of Veterinary and Animal Science, University of Massachusetts, Amherst, MA, USA
Iris Thesmar:
lthesmar@umass.edu
Molecular and Cellular Biology Program, University of Massachusetts, Amherst MA, USA
Department of Veterinary and Animal Science, University of Massachusetts, Amherst, MA, USA
Julia Cernjul:
Jcernjul@umass.edu
Department of Veterinary and Animal Science, University of Massachusetts, Amherst, MA, USA
Xinjian He:
xinjianhe@umass.edu
Animal Biotechnology and Biomedical Sciences Program, University of Massachusetts, Amherst, MA, USA
Department of Veterinary and Animal Science, University of Massachusetts, Amherst, MA, USA
Jesse Mager:
jmager@umass.edu
Department of Veterinary and Animal Science, University of Massachusetts, Amherst, MA, USA
Wei Cui:
wcui@umass.edu
Department of Veterinary and Animal Science, University of Massachusetts, Amherst, MA, USA
Animal Models Core Facility, Institute for Applied Life Sciences (IALS), Amherst, MA, USA
Dominique Alfandari:
alfandar@vasci.umass.edu
Department of Veterinary and Animal Science, University of Massachusetts, Amherst, MA, USA
Elena L. Pobezinskaya:

pobeinskaya@umass.edu
Department of Veterinary and Animal Science, University of Massachusetts, Amherst, MA, USA
Leonid A. Pobezinsky:
lpobezinsky@umass.edu
Department of Veterinary and Animal Science, University of Massachusetts, Amherst, MA, USA

ONE-SENTENCE SUMMARY:

Naïve Dapl1 positive CD8 T cells include a pre-programmed subset biased toward differentiation into memory-like T cells.

SUMMARY

Memory CD8 T cells play a vital role in providing lasting immune protection, yet their origins remain incompletely understood. Contrary to classical models, emerging evidence suggests that heterogeneity within the naïve T cell pool may influence fate decisions prior to antigen encounter. However, the markers of naïve T cell heterogeneity have not yet been clearly defined. Here, we describe intraclonal heterogeneity within the naïve T cell population marked by the protein Dapl1. Using novel monoclonal antibodies and a reporter-knockout mouse model, we found that Dapl1-positive naïve CD8 T cells exhibit distinct phenotypes compared to their Dapl1-negative counterparts. Furthermore, this population includes a subset of pre-programmed precursors biased toward memory lineage fate. The differentiation of these precursors is independent of Dapl1 but relies on the transcription factor Bcl11b, resulting in the generation of Dapl1-positive central memory-like CD8 T cells in response to infection, and stem-like memory cells in response to cancer. Notably, naïve Dapl1-positive T cells originate among mature thymocytes and gradually appear in the periphery within several days after birth. Our findings suggest that committed memory precursors in the Dapl1-positive population may represent an alternative pathway for memory CD8 T cell generation, offering new avenues for therapeutic application.

INTRODUCTION

CD8 T lymphocytes are indispensable for immune defense, targeting and eliminating host cells infected with intracellular pathogens or transformed by cancer. After antigen clearance, most effector cytotoxic T lymphocytes (CTLs) undergo apoptosis, with only a small fraction persisting as memory CD8 T cells. These memory cells play critical roles in long-term immune protection, rapidly responding to antigen re-exposure, and are central to tumor immunotherapies, including adoptive T cell transfer, CAR-T therapy, and checkpoint blockade [1-16]. Furthermore, memory CD8 T cells are essential for the efficacy of vaccines, making their study important for advancing immunotherapies and vaccine development.

Although much progress has been made, the molecular mechanisms underlying memory CD8 T cell differentiation remain incompletely understood. Two competing models have sought to explain memory T cell ontogeny. The “linear” model suggests that memory cells arise from effector cells, while the “bifurcative” model suggests that asymmetric division of activated CD8 T cells generates distinct effector and memory lineages [17-27]. Despite their differences, both models share the assumption that memory fate is determined during antigen-driven differentiation in the immune response. Recent findings, however, challenge this paradigm, suggesting that heterogeneity within the naïve T cell population may predetermine memory or effector potential before antigen stimulation [28-39]. Progress in this area remains hindered by the absence of reliable markers to identify such heterogeneity, highlighting the need for innovative approaches to unravel the origins of memory CD8 T cells.

Here, we report a new marker Death Associated Protein Like-1 (Dapl1), the expression of which reveals the heterogeneity of naïve T cells. The *Dapl1* gene encodes a 108 amino acid intracellular protein with predicted localization in the cytoplasm. Although very little is known about Dapl1 protein function, it has been reported that Dapl1 may interact with many major pathways including MYC-, MAPK-, NFκb- and NFAT-cascades [40-45]. Furthermore, in other models, Dapl1 is portrayed as a potential “gate keeper” of stem-like phenotypes, suppressing generation of reactive oxygen

130 species and protein translation [46,47]. It has been demonstrated that Dapl1 is highly expressed in
131 skin, retina, and testis. Furthermore, the *Dapl1* gene appeared among the top differentially
132 expressed genes (DEGs) in stem-like memory CD4 and CD8 T cells in many recent studies [15,48-
133 63]. The generation of anti-Dapl1 monoclonal antibodies and a Dapl1-reporter mouse model
134 enabled us to detect and study Dapl1-expressing T cells. With these tools, we identified a distinct
135 subpopulation of Dapl1+ cells within naïve T lymphocytes, revealing an additional layer of
136 heterogeneity. Furthermore, we found that within Dapl1+ CD8 T cells, a subset of pre-
137 programmed lymphocytes preferentially differentiates into memory-like cells during immune
138 responses to pathogens and cancer. Thus, our findings uncover a complementary mechanism
139 contributing to memory formation in CD8 T cells.
140

141 **RESULTS**

142 **1. Dapl1 expression reveals heterogeneity of naïve T cells.**

143 Previously, we demonstrated that the expression of let-7 miRNAs significantly promotes
144 generation of memory CD8 T cells[15]. We found that the evolutionarily conserved *Dapl1* gene is
145 among the top DEGs between let-7-transgenic (Let-7Tg) and let-7-deficient (Let-7KD) cytotoxic T
146 lymphocytes (CTLs). Let-7Tg CTLs with memory potential expressed very high levels of *Dapl1*
147 mRNA, while terminally differentiated Let-7KD CTLs had almost none (Fig. 1A).
148 Based on ImmGen RNA-seq data sets [64], we have found that *Dapl1* mRNA expression is restricted
149 to peripheral naïve T cells and also persists at lower levels in memory precursors (MPECs) and
150 memory CD8 T cells, but is not present in short lived effector cells (SLECs) (Fig. 1B). Furthermore,
151 recent publications have shown the association of *Dapl1* expression with stem-like memory
152 phenotypes for both CD4 and CD8 T cell lineages [15,48-63]. We hypothesized that the Dapl1
153 expression pattern may reflect the gradual loss of multipotent traits of naïve T cells during
154 differentiation into effector cells. Therefore, Dapl1 is a candidate marker for tracing memory
155 lineage cells, where such traits are still preserved.

156 To detect Dapl1-expressing cells, we generated our own monoclonal antibody (mAb) against the
157 mouse Dapl1 protein (clone 6H9). The specificity of this anti-Dapl1 mAb was validated by enzyme-
158 linked immunosorbent assay (ELISA) using recombinant protein and by Western blot (WB) with
159 Dapl1-transduced NIH 3T3 cells (fig. S1, A and B). The 6H9 mAb identified a 12 kDa band
160 corresponding to Dapl1 protein in both CD4 and CD8 T cells from wild-type (WT) mice by WB,
161 but no Dapl1 expression was detected in thymocytes (Fig. 1C), recapitulating the mRNA
162 expression patterns (Fig. 1B). Using the 6H9 mAb for confocal microscopy, we confirmed the
163 predicted cytoplasmic localization of Dapl1 within the cells (Fig. 1D and fig. S1C). Unexpectedly,
164 we observed that not all CD8 T cells were Dapl1-positive. In fact, intracellular (IC) staining for flow
165 cytometry revealed that only 30-50% of naïve peripheral T cells expressed Dapl1 (Fig. 1, E and
166 F). Notably, the intensity of Dapl1 expression and the frequency of Dapl1+ cells were higher in
167 CD8 T cells than in CD4 T cells (Fig. 1F). We also observed that the proportion of Dapl1+
168 lymphocytes and their expression levels of Dapl1 were slightly elevated in blood compared to the
169 spleen and lowest in lymph nodes. We next compared the phenotype of Dapl1+ and Dapl1- T
170 cells based on the expression of selected surface markers for naïve and activated T cells (fig.
171 S1D). Uniform manifold approximation and projection (UMAP) analysis of multicolor flow
172 cytometry data revealed that Dapl1+ T cells clustered separately from Dapl1- T lymphocytes for
173 both CD4 and CD8 populations (Fig. 1G). Furthermore, the majority of Dapl1+ CD4 and CD8 T
174 cells exhibited quiescent $CD44^{low}CD122^{low}$ phenotypes and had fewer activated CXCR3+ cells
175 compared to their Dapl1- counterparts (Fig. 1H). In addition, gated naïve ($CD44^{low}CD62L^{hi}$)
176 Dapl1+ CD8 T cells contained a high frequency of Ly6C+ cells and expressed elevated levels of
177 CD5, CD44, CD62L, CD127, and CD122 compared to naïve Dapl1- cells (Fig. 1I and fig. S1, E
178 and F). In contrast, naïve Dapl1+ CD4 T cells exhibited a milder phenotype, characterized by
179 increased expression of CD5 and CD127. Thus, Dapl1 expression uncovers previously
180 unrecognized heterogeneity within the naïve CD4 and CD8 T lymphocyte populations.
181

182 **2. Dapl1-reporter model uncovers heterogeneity among many T cell subsets.**

183 To investigate the properties of Dapl1+ T cells, we generated a Dapl1-reporter mouse model,
184 Dapl1^{ZsG}, in which the fusion construct of Dapl1, self-cleaving P2A peptide, and fluorescent
185 protein ZsGreen (ZsG) is expressed under the control of the *Dapl1* gene's promoter and all its
186 regulatory elements (Fig. 2A). Overall, the mice appeared phenotypically identical to littermate
187 controls. At steady state, 20-30% of CD4 and 40-50% of CD8 peripheral T cells in Dapl1$^{ZsG/WT}$
188 mice were ZsG+ (Fig. 2B). Moreover, the intensity of ZsG expression and the frequency of ZsG+
189 lymphocytes were higher in CD8 T cells than in CD4 T cells. This expression pattern of ZsG
190 correlates well with Dapl1 mRNA (Fig. 1B) and protein (Fig. 1E) expression in WT T lymphocytes.
191 Unexpectedly, we discovered that the *Dapl1^{ZsG}* allele does not result in production of Dapl1
192 protein, despite mRNA expression (Fig. 2C and fig. S2A). It is possible that extra amino acids
193 from the P2A peptide modify the C-terminus of Dapl1 protein leading to its instability. We
194 confirmed this by overexpressing N- and C-terminal HA-tagged Dapl1 constructs (fig. S2B), where
195 only the N-terminal HA-tag was well tolerated. Thus, serendipitously, we created a *Dapl1^{ZsG}*
196 knockout-reporter allele. By leveraging this model, we utilized heterozygous Dapl1$^{ZsG/WT}$ mice as
197 reporters, with ZsG marking Dapl1-expressing cells. In contrast, homozygous Dapl1$^{ZsG/ZsG}$ mice,
198 which lack Dapl1 expression, allowed us to track "Dapl1-wannabe" cells through ZsG expression.
199 In Dapl1$^{ZsG/WT}$ mice, ZsG expression was restricted to T cells (Fig. 2D and fig. S2C). While TCR$\alpha\beta$
200 T cells in secondary lymphoid organs contained a large proportion of ZsG+ cells, few TCR$\gamma\delta$ T
201 cells and virtually no NKT lymphocytes expressed ZsG. Using double reporter
202 Dapl1$^{ZsG/WT}$Foxp3$^{RFP/RFP}$ mice, we found that CD4 Foxp3+ T regulatory cells (Tregs) contained only
203 2-5% of ZsG+ cells, while a rare population of CD8 Foxp3+ Tregs had approximately 20% ZsG+
204 cells (Fig. 2E and F). Notably, the presence of ZsG+ T cells was comparable between splenic and
205 liver T cell subsets but sharply reduced in the small intestine for both innate-like and conventional
206 populations (Fig. 2, G and H, fig. S3, A and B, and fig. S4, A to D). In the colon, innate-like T

207 lymphocytes were predominantly ZsG-, whereas conventional T cells contained 20-30% of ZsG+
208 cells, highlighting the tissue-specific distribution of Dapl1-expressing cells.
209 Next, we investigated the phenotype of conventional and regulatory ZsG+ T cells from
210 Dapl1$^{ZsG/WT}$Foxp3$^{RFP/RFP}$ mice. As expected, the conventional (Foxp3-) ZsG+ CD4 and ZsG+ CD8
211 T cells closely phenocopied WT Dapl1+ T cells stained with anti-Dapl1 mAb (Fig. 1F, Fig. 3, A to
212 C, and fig. S5, A to C). The majority of ZsG+ T cells were quiescent and, when gated on the naïve
213 (CD44^{low}CD62L^{hi}) population, exhibited significantly elevated levels of CD5, CD44, CD62L,
214 CD127 and CD122. Similar to Dapl1+ cells from WT mice, ZsG+ CD8 T cells were enriched with
215 Ly6C+ cells. Interestingly, ZsG+Foxp3+ CD4 Tregs displayed reduced surface expression of CD5
216 and CD44, an increased proportion of CD62L+ and Ly6C+ cells, and a lower frequency of PD-1+
217 cells (fig. S5, D and E). This phenotype may indicate that Dapl1+ Tregs have a less activated
218 state, which has been previously linked to reduced suppressive function [65-67]. Altogether, our
219 results confirmed that ZsG reliably reports Dapl1+ subpopulations of both CD4 and CD8 T cells
220 in Dapl1$^{ZsG/WT}$ mice.
221 To test whether the heterogeneity of Dapl1 expression is due to differences in T cell receptor
222 (TCR)-specificity, we generated two different TCR-transgenic mice (P14 and OT-I) on a
223 Dapl1$^{ZsG/WT}$Rag2$^{-/-}$ background. Based on ZsG expression, we found that similar to polyclonal
224 CD8 T cells, approximately 40% of both naïve P14 and OT-I CD8 T cells expressed Dapl1 (Fig.
225 3D) revealing intraclonal heterogeneity of naïve CD8 T cells. Reanalysis of existing scRNA-seq
226 datasets for naïve P14, OT-I, and polyclonal cells confirmed the presence of both Dapl1+ and
227 Dapl1- CD8 T cells at the mRNA level (Fig. 3E). Furthermore, these cells exhibited markedly
228 different transcriptomes, indicating the presence of two distinct populations (Fig. 3E). Notably,
229 naïve Dapl1+ CD8 T cells upregulated a unique set of genes associated with cytokine signaling,
230 interferon signaling, and immunoregulation, while downregulating genes involved in differentiation
231 and apoptosis [68-73] (Fig. 3F). Together, these findings highlight significant heterogeneity of different
232 T cell subsets even within monoclonal naïve populations.

233

234 **3. Dapl1+ CD8 T cells have biased differentiation towards memory lineage.**

235 Naïve Dapl1+ and Dapl1- CD8 T cells exhibited significant differences in their phenotype and
236 transcriptional profiles. Therefore, we investigated whether Dapl1+ and Dapl1- naïve CD8 T cells
237 are two separate lineages with unique differentiation potentials. First, we tested the persistence
238 of Dapl1 expression in CTLs generated from bulk naïve P14 CD8 T cells. Based on both
239 endogenous expression of Dapl1 protein in WT mice and ZsG in our reporter, we observed that
240 only a small fraction of differentiated cells were Dapl1+ (Fig. 4, A and B, and fig. S6, A and B).
241 Next, we examined the phenotype of Dapl1+ and Dapl1- CTLs, using the expression of CD62L
242 as a proxy of memory lineage and Tim-3 for terminally differentiated effector cells[15]. Surprisingly,
243 most Dapl1+ CTLs displayed a memory-like (CD62L+Tim3-) phenotype and expressed low levels
244 of effector markers such as CD44, CD122, CD160, PD-1 and 2B4. In contrast, Dapl1- CTLs
245 showed significantly higher expression of these molecules and also included a population of
246 terminally differentiated (CD62L-Tim3+) cells. Furthermore, we found that the frequency of
247 ZsG+(Dapl1+) CTLs increased after treatment with rapamycin, a potent inhibitor of TORC1 known
248 to promote the formation of memory cells [74] (Fig. 4C). These results indicate that Dapl1 expression
249 in differentiating cells may be associated with memory formation.

250 The small number of Dapl1+ CTLs may indicate that many cells downregulated Dapl1 expression
251 during the differentiation process. To test this, we generated CTLs *in vitro* from sorted
252 ZsG+(Dapl1+) and ZsG-(Dapl1-) naïve CD8 T cells from P14+Dapl1$^{ZsG/WT}$Rag2$^{-/-}$ mice. Indeed,
253 many initially Dapl1+ cells lost the expression of Dapl1 (Ex-Dapl1) during CTL differentiation and
254 were phenotypically similar to CTLs derived from naïve ZsG-(Dapl1-) cells. In contrast, the small
255 proportion of CTLs that retained ZsG expression had exclusively memory-like phenotypes
256 (CD62L+Tim3-) with reduced levels of effector markers (fig. S6C). Of note, the vast majority of
257 effector descendants of naïve ZsG-(Dapl1-) T cells remained Dapl1-, suggesting limited plasticity
258 from Dapl1- to Dapl1+ subpopulations during differentiation.

259 To directly investigate the fate of differentiating Dapl1+ and Dapl1- CD8 T cells, we employed an
260 *in vivo* infection mouse model, where we used *Listeria monocytogenes* that expressed the GP33
261 peptide (LM-GP33), a cognate antigen for P14 TCR-transgenic CD8 T cells. Sorted Dapl1+ and
262 Dapl1- naïve P14 T cells were separately injected into LM-infected host mice and their phenotypes
263 were assayed over time (Fig. 4, D and E). During the immune response, many initially Dapl1+
264 cells lost Dapl1 expression, becoming Ex-Dapl1 cells, which confirmed our *in vitro* observations.
265 Importantly, the frequency of Dapl1+ cells gradually recovered, with the majority of long-lived
266 memory cells expressing Dapl1. On day 7 and 14 post-infection, CD8 T cells that retained Dapl1
267 expression (ZsG+) had acquired an MPEC phenotype (KLRG1-CD127+), whereas Ex-Dapl1 cells
268 differentiated into both MPECs and SLECs (KLRG1^{+}CD127^{-}). Notably, Ex-Dapl1 cells were
269 enriched with double-positive (KLRG1+CD127+) effectors, which have the potential to generate
270 diverse memory subsets, including effector memory T cells (T_{EM}, CD44^{hi}CD62L-) [75]. After 30 days
271 post-infection, most of the Dapl1+ memory cells exhibited the phenotype of central memory CD8
272 T cells (T_{CM}, CD44^{hi}CD62L+). In contrast, Ex-Dapl1 memory cells, in addition to T_{CM} population,
273 contained a significantly higher proportion of T_{EM} cells. Overall, the number of generated memory
274 cells was comparable between descendants of Dapl1+ and Dapl1- naïve T cells (fig. S6D). Of
275 note, the differentiated progeny of Dapl1- naïve CD8 T cells remained preferentially ZsG-(Dapl1-
276) at all times and gave rise to both SLECs and MPECs as expected. In this case, the appearance
277 of a very small proportion of Dapl1+ memory cells (2-4%) can be explained by initial sort impurity
278 or a very limited generation of Dapl1+ lymphocytes *de novo*. We also noticed that in both *in vitro*
279 and *in vivo* experiments, cells which retained expression of Dapl1 expressed higher surface levels
280 of CD62L than their Dapl1- counterparts (fig. S6, C and E), suggesting that Dapl1+ and Dapl1-
281 memory lineage cells may be different. To this end, we reanalyzed publicly available scRNA-seq
282 datasets for P14 T_{CM}, T_{EM}, and resident memory (T_{RM}) cells generated in response to acute
283 Lymphocytic Choriomeningitis Virus Armstrong (LCMV-Arm) infection [62,68,70,71,76,77]. We confirmed
284 that a proportion of Dapl1+ cells is present in T_{CM} but not T_{EM} or T_{RM} populations after acute LCMV-

285 Arm infection [68] (fig. S6F). Furthermore, upregulated DEGs in Dapl1+ T_{CM} cells included genes
286 associated with stem-like memory cell differentiation (*Lef1, Id3, Sell, Ccr7 and etc.*) and those
287 involved in the regulation of translation and survival (Fig 4F and fig. S6G), while the genes linked
288 to leukocyte activation were downregulated. These data demonstrate that differentiated Dapl1+ T
289 cells are transcriptionally different from Dapl1- counterparts and express higher levels of key
290 memory related genes. Overall, our results suggest that the pool of Dapl1+ naïve CD8 T cells
291 harbors a distinct subpopulation pre-committed to memory lineage, with their progeny marked by
292 persistent expression of Dapl1 and unique transcriptional profile. This finding indicates that, for a
293 subset of naïve CD8 T cells, memory fate may be pre-determined prior to antigen encounter (fig.
294 S7A).
295 To define the mechanisms regulating Dapl1+ CD8 T cell differentiation, we focused on the
296 transcription factors (TFs) that were upregulated in Let-7Tg CTLs where Dapl1 was also strongly
297 expressed [15]. Specifically, we tested the ability of selected TFs (Bcl11b, Klf2, Tcf1, Lef1, Sox4,
298 Bach2, Foxo1, and Id3) from memory signature genes of Let-7Tg CTLs, to support the
299 differentiation of Dapl1+ CTLs *in vitro*. Compared to the empty-retrovirus (RV) control, WT CTLs
300 transduced with RVs encoding *Bcl11b*, *Klf2*, and *Tcf7* showed robust generation of Dapl1+ CTLs
301 (Fig. 4G and fig. S8A). In addition to Dapl1 expression, these transduced CTLs also exhibited
302 increased frequency of CD62L+ cells and decreased frequency of Tim3+ cells (Fig. 4G and fig.
303 S8A). In contrast, CTLs transduced with Id2, a TF involved in effector cell differentiation, failed to
304 generate Dapl1+ cells. Given the fact that Bcl11b was the most potent inducer of Dapl1+ CTLs *in*
305 *vitro* and has been previously implicated in the formation of MPECs and CD8 T memory cells [78,79],
306 we next assessed the expression of Dapl1 in WT and Bcl11b$^{-/-}$ MPECs generated in response to
307 LM-OVA infection using a publicly available RNA-seq dataset [79]. On day 9 post infection (dpi), in
308 addition to compromised cell numbers [79], Bcl11b$^{-/-}$ MPECs had significantly reduced expression
309 of Dapl1 mRNA compared to WT cells (fig. S8B), while as expected, all SLECs had low Dapl1

310 expression. Altogether, these results suggest that the transcription factor Bcl11b promotes the
311 differentiation of Dapl1+ memory lineage CD8 T cells.
312 During chronic infection or cancer, effector cells become exhausted (T_{EX}) and the formation of
313 memory cells is altered leading to the generation of a distinct memory lineage known as
314 progenitors of exhausted cells (T_{PEX}) with stem-like potential [3,6-8,16]. Importantly, these stem-like
315 cells are the primary responders to various tumor treatments including immunotherapies such as
316 T cell adoptive transfer, CAR-T, and checkpoint blockade. Phenotypically, T_{PEX} express CD62L,
317 Ly108 and low levels of inhibitory receptors like Tim-3 on their surface [3]. We therefore investigated
318 the presence and phenotype of differentiated Dapl1+ T cells within the tumor microenvironment
319 using B16 melanoma mouse model. Approximately 10-20% of CD8 tumor infiltrating lymphocytes
320 (TILs) isolated from Dapl1$^{ZsG/WT}$ or WT B16-bearing mice were Dapl1+. These cells were antigen
321 experienced (CD44^{hi}) and displayed the T_{PEX} phenotype (CD62L+Tim-3- and Ly108^{hi}) (fig. S9, A
322 to C). The reanalysis of available TILs scRNA-seq dataset further confirmed our findings that T_{PEX}
323 but not terminally differentiated T_{EX} cells contain a Dapl1+ population [50] (fig. S9E). Furthermore,
324 the upregulated DEGs in Dapl1+ CD8 TILs included genes that are linked to a stem-like memory
325 cell profile (*Lef1, Klf2, Myb, Sell, Slamf6 and etc.*), cell differentiation, translation and survival
326 [6,11,50,80-82] (fig. S9F). These data suggest that during anti-tumor immune responses, a pre-
327 committed subpopulation of naïve Dapl1+ cells also exhibits differentiation bias and contributes
328 to the formation of stem-like memory CD8 T cells in TILs.
329

330 **4. Dapl1 expression is not required for the differentiation of Dapl1+ memory CD8 T cells**
331 **but may contribute to their maintenance and cytokine production.**

332 Whether Dapl1 plays a role in the differentiation of memory CD8 T cells is unknown. To explore
333 this question, we took advantage of our mouse model, where homozygosity of the Dapl1-reporter
334 allele results in Dapl1 deficiency (Fig. 2C). In Dapl1$^{ZsG/ZsG}$ mice, ZsG expression serves as a
335 marker for Dapl1-deficient T cells, allowing us to track and characterize these “wannabe” cells.

336 After adoptive transfer of naïve Dapl1$^{WT/WT}$ or Dapl1$^{ZsG/ZsG}$ P14 T cells followed by LM-GP33
337 infection, we consistently observed a mild but significant decrease in the proportion of Dapl1-
338 wannabe cells at every stage of the immune response including formation of memory cells (Fig.
339 5A), while the phenotype of Dapl1-wannabes resembled the memory lineage phenotype of
340 Dapl1+ cells (Fig. 5B and fig. S10A). We obtained similar results in differentiation experiments *in*
341 *vitro* (fig. S10B). Of note, loss of Dapl1 expression had no impact on the generation of Dapl1-
342 wannabe TILs or their stem-like memory phenotype in Dapl1$^{ZsG/ZsG}$ mice (fig. S10C). Furthermore,
343 in a separate *in vivo* experiment the phenotype of differentiating CD8 T cells transduced with
344 Dapl1-RV was indistinguishable from that of cells transduced with an empty-RV control, indicating
345 that Dapl1 overexpression does not affect the lineage fate of CD8 T cells (fig. S10D). Thus, our
346 results suggest that Dapl1 may be involved in maintenance of differentiating cells rather than the
347 control of their fate.
348 We next sought to test functional differences between Dapl1+ and Dapl1 wannabe memory CD8
349 T cells. Restimulation of memory cells collected 30+ days post infection demonstrated that true
350 Dapl1 positive memory CD8 T cells contained a higher proportion of polyfunctional (Ifnγ+Tnfα+)
351 cells compared to Dapl1-wannabe or Dapl1- memory T cells (Fig. 5C). However, adoptively
352 transferred sorted P14 Dapl1$^{WT/WT}$ and Dapl1$^{ZsG/ZsG}$ memory T cells control B16-GP33 tumor
353 growth with similar efficiency in tumor-bearing mice suggesting that the absence of Dapl1 does
354 not affect the overall performance of memory T cells (fig. S10E). Additionally, although a previous
355 report suggests that mice with a global CRISPR-mediated knockout of Dapl1 exhibit enhanced
356 effector function of CD8 T cells in anti-tumor immune responses [45], we did not observe differences
357 in MC38 tumor growth control between Dapl1$^{ZsG/ZsG}$ and Dapl1$^{WT/WT}$ mice, pointing to potential
358 discrepancies between these two models of Dapl1-deficiency (fig. S10F). Collectively, our findings
359 suggest that while Dapl1 is dispensable for the generation and function of memory CD8 T cells,
360 it contributes to the maintenance of memory lineage cells and production of effector cytokines.
361

362 **5. The development of naïve Dapl1+ T cells.**

363 Previous studies have shown that neonatal CD8 T cells exhibit reduced memory potential and
364 tend to differentiate into SLECs rather than MPECs or memory cells [34,83,84]. Based on this, we
365 hypothesized that the development of Dapl1+ T cells may be limited in neonatal mice. To test this,
366 we assessed the frequency of naïve Dapl1+ T cells in the spleens of Dapl1$^{ZsG/WT}$ mice at one day,
367 one week, and one month after birth. In one-day-old neonatal mice, no Dapl1+ T cells were
368 detected in the periphery. However, these cells gradually appeared with age (Fig. 6A), suggesting
369 a developmental delay in generating Dapl1+ T cells during the neonatal period.

370 We then examined whether Dapl1+ T lymphocytes originate within the thymus before populating
371 secondary lymphoid organs or if they arise directly in peripheral tissues. In the adult thymus, we
372 detected a small population of Dapl1+ cells only among mature CD4 and CD8 single positive (SP)
373 thymocytes (Fig. 6B and fig. S11A). To confirm these findings, we analyzed Dapl1 mRNA levels
374 in a bulk RNA-seq dataset of sorted thymocyte populations at different developmental stages [85].
375 The results corroborated that only post-selected thymocytes expressed Dapl1 (Fig. 6C).
376 Additionally, projecting Dapl1 expression on pseudotime analysis of a thymocyte scRNA-seq
377 dataset indicated that Dapl1 mRNA expression is indeed upregulated in a subset of the most
378 mature thymocytes [86] (Fig. 6D).

379 To investigate whether the mature Dapl1+ T cells found in the thymus could originate from
380 recirculation from the periphery, we utilized CD24 as a marker of thymocyte maturation. The
381 surface expression of CD24 is highest on immature thymocytes and declines with maturation,
382 while peripheral T cells are generally CD24-negative. We observed that ZsG+(Dapl1+) TCR+CD8
383 thymocytes exhibited intermediate levels of CD24 – lower than immature double-positive
384 thymocytes but significantly higher than peripheral T cells from lymph nodes (Fig. 6E), suggesting
385 their thymic origin. Moreover, the lower CD24 expression on ZsG+(Dapl1+) TCR+CD8
386 thymocytes compared to mature ZsG-(Dapl1-) TCR+CD8 thymocytes indicated that Dapl1+ cells
387 represent a more advanced maturation stage. Lastly, ZsG intensity was lower in Dapl1+

388 thymocytes than peripheral T cells (Fig. 6F), altogether ruling out recirculation from the periphery
389 as a likely source.
390 The presence of Dapl1+ T cells among the most mature thymocytes implies that single-positive
391 thymocytes upregulate Dapl1 immediately before exiting the thymus, potentially explaining the
392 low frequency of Dapl1+ cells in thymus relative to peripheral lymphoid organs. To test this, we
393 blocked T cell egress from the thymus using FTY720, a potent agonist of S1PR1 receptor that is
394 involved in T cell migration [87]. After one week of FTY720 treatment, we observed a significant
395 increase in the proportion of ZsG+(Dapl1+) T cells among mature SP4 and SP8 populations in
396 Dapl1$^{ZsG/WT}$ mice (Fig. 6G), while peripheral ZsG+(Dapl1+) T cell frequency remained unchanged
397 (fig. S11B). Together, these findings demonstrate that Dapl1+ T cells first emerged among mature
398 thymocytes shortly before their exit into peripheral lymphoid organs, highlighting the thymus's
399 potential role in pre-programming naïve T cell populations.
400
401 **Discussion**
402 Understanding the origins of memory T cells has been a key focus in immunology. It is generally
403 accepted that the steps leading to memory lineage commitment occur after antigen recognition.
404 Consequently, naïve T cells have been regarded as precursors capable of differentiation into
405 memory and effector cells during immune responses. This bipotential ability was elegantly
406 demonstrated in adoptive transfer experiments of single naïve CD8 T cells [19,21,26]. These and many
407 other findings support the most popular model of memory formation proposed by Steven Reiner's
408 group, where naïve T cells undergo asymmetric division after antigen encounter, producing one
409 daughter cell committed for the effector lineage and another for the memory lineage [20,22,27]. Here,
410 we report a discovery of a novel subpopulation of naïve CD8 T cells whose differentiation does
411 not align with the conventional model of memory formation. These naïve cells are already pre-
412 committed to differentiate into memory-like lineage cells even before encountering an antigen.

413 They can be identified by persistent expression of the *Dapl1* gene during differentiation, both *in*
414 *vitro* and *in vivo*.
415 Using in-house monoclonal antibody (6H9) against the Dapl1 protein and a Dapl1-reporter mouse
416 model, we uncovered significant heterogeneity among naïve T cells based on Dapl1 expression.
417 At steady state, most of Dapl1+ T cells had a true naïve phenotype and were largely excluded
418 from activated or differentiated subsets. However, they also exhibited distinct features, including
419 slightly elevated levels of CD5, CD44, CD62L, CD122 and CD127 (in CD8 T cells), upregulated
420 expression and frequency of Ly6C, and reduced CD103. This heterogeneity was also observed
421 in naïve CD8 T cells from MHC class I restricted TCR-transgenic mice, indicating previously
422 unrecognized intraclonal diversity. Furthermore, scRNA-seq analysis of multiple data sets of naïve
423 CD8 T cells revealed a unique transcriptional signature of Dapl1+ lymphocytes, further supporting
424 their distinct identity within the naïve T cell pool.
425 Intriguingly, during the immune response, a small subset of naïve Dapl1+ CD8 T cells retained
426 Dapl1 expression and differentiated into central memory T cells. Notably, naïve Dapl1- cells
427 neither upregulated Dapl1 nor exhibited any bias in their differentiation. These findings strongly
428 suggest that within the Dapl1+ naïve CD8 T cell population, a small population (10-20%) is pre-
429 committed to the memory lineage even before antigen stimulation. This previously unrecognized
430 pathway of memory formation adds more complexity to the current model of CD8 T cell
431 differentiation, which is based on the fact that memory lineage commitment occurs only after
432 antigen exposure [17]. Although the pre-programming of naïve CD8 T cells into memory has not
433 been previously described, the dominance of the bifurcative model has been challenged by a few
434 other findings. For instance, nuclear envelope invaginations have been shown to distinguish naïve
435 CD8 T cells predisposed to differentiate into effector-like cells [30]. Similarly, type-I IFN exposure in
436 naïve CD4 T cells caused a bias toward central memory cell differentiation by influencing their
437 transcriptional and functional programming [28]. Additionally, biased differentiation has been
438 observed between naïve $CD5^{high}$ and $CD5^{low}$ CD4 T cells [33].

439 We found that Dapl1 expression in differentiated cells is associated with the CD8 T cell subsets
440 possessing memory potential, including memory precursors, central memory cells and stem-like
441 cells. This observation aligns with prior studies in which Dapl1 was identified among top DEGs in
442 memory-like lymphocytes [15,48-63]. Furthermore, the transcriptional difference between Dapl1+ and
443 Dapl1- memory cells revealed a new layer of heterogeneity. This raises the possibility that
444 differentiated Dapl1+ lymphocytes represent a novel lineage of memory CD8 T cells. It is
445 important to mention that even Ex-Dapl1 cells, which lost the expression of Dapl1 during
446 differentiation, were enriched with KLRG1+CD127+ memory precursors. Further research is
447 needed to determine whether these phenotypic differences translate into functional variations and
448 to identify additional markers that can reliably pinpoint memory precursors within the Dapl1+ naïve
449 T cell population.
450 The general biological function of the Dapl1 protein remains largely unexplored. In lower
451 vertebrates such as zebrafish and *Xenopus*, the homologous Dap1b protein functions as a
452 translational inhibitor by directly interacting with ribosomes, rendering them dormant and
453 contributing to ribosomal storage and translational repression [46]. In mammals, Dapl1 has been
454 primarily studied outside the immune system [40-44,47], though one study implicated it in the negative
455 regulation of anti-tumor activity of CD8 T cells [45]. Using our homozygous reporter mouse model,
456 we investigated Dapl1-deficient lymphocytes but did not observe enhanced anti-tumor activity.
457 Instead, we found that Dapl1 expression influences the frequency of Dapl1+ memory CD8 T cells
458 and their production of effector cytokines such as IFNγ and TNFα. Further research is required to
459 elucidate the molecular mechanisms through which Dapl1 drives these observed phenotypes.
460 Among the transcription factors known to promote memory formation, Bcl11b emerged as the
461 most potent in supporting the differentiation of Dapl1+ memory lineage cells *in vitro* and *in vivo*.
462 This aligns with previous studies showing that, beyond its essential role in T cell lineage
463 specification, Bcl11b is required for memory CD8 T cell differentiation and counteracts the innate-
464 effector program [78,79,88]. However, the precise role of Bcl11b in this process remains unclear,

465 including whether it directly regulates Dapl1 expression. Given the critical role of Bcl11b in T cell
466 development, future investigation should determine whether its expression is necessary for the
467 formation of naïve Dapl1+ T cells and whether it contributes to pre-programming of memory
468 precursors within this population.

469 Although most Dapl1+ naïve T cells are located in the periphery, our findings demonstrate that
470 the earliest Dapl1+ naïve T cells can be detected among the most mature thymocytes, suggesting
471 a thymic developmental origin. However, the signals driving the development of Dapl1+ cells in
472 the thymus remained unidentified. It is also unclear whether the memory commitment observed
473 in a subset of Dapl1+ naïve T cells occurs in the thymus or in the periphery. Addressing these
474 questions is of significant interest, as it could inform strategies to enhance vaccine efficiency and
475 improve T cell-based therapies.

476 Furthermore, we found that the development of Dapl1+ T cells is age-dependent. Peripheral
477 Dapl1+ T cells emerge gradually within the first week after birth, coinciding with the transition of
478 the neonatal immune system to an adult-like state. This transition is thought to be governed by a
479 postnatal switch in the source of hematopoietic stem cells (HCSs): from embryonic HSCs derived
480 from liver to adult HSCs originated in the bone marrow [89]. Notably, neonatal CD8 T cells are
481 reported to have diminished memory potential, favoring differentiation into short-lived effector
482 cells [34,83,84]. This process is largely mediated by the transient expression of Lin28b, an RNA-
483 binding protein that inhibits the biogenesis of evolutionary conserved let-7 miRNAs [90,91]. Although
484 Lin28b-transgenic CTLs (Let-7KD) lack detectable *Dapl1* mRNA expression (Fig. 1A), it remains
485 to be determined whether Dapl1 expression is regulated by let-7.

486 In summary, our study predicts the existence of a novel subpopulation within a pool of Dapl1+
487 naïve CD8 T cells that appears pre-committed to differentiate into memory-like cells even before
488 antigen exposure. Moreover, we demonstrated that Dapl1 expression serves as a valuable marker
489 for tracking the progeny of this population among long-lived cells generated during immune
490 responses to cancer or infection. Future investigations are needed to elucidate the precise roles

491 these cells play in immunity and to uncover the molecular mechanisms underpinning their
492 commitment to memory lineage.
493
494
495
496
497
498
499
500
501
502
503
504
505
506
507
508
509
510
511
512
513
514
515
516

517 **Materials and methods**

518 Ethics statement

519 This study was performed in accordance with the recommendations in the Guide for the Care and
520 Use of Laboratory Animals of the National Institutes of Health. All animals were handled according
521 to approved institutional animal care and use committee (IACUC) protocols of the University of
522 Massachusetts, Amherst.

523 Animals

524 B6 (C57BL/6J, stock # 000664), *Rag2*$^{-/-}$ (B6.Cg-*Rag2*$^{tm1.1Cgn}$/J, stock # 008449), OT-I (C57BL/6-
525 Tg(TcraTcrb)1100Mjb/J), stock # 003831) and FoxP3^{RFP} (C57BL/6-*Foxp3*^{tm1Flv}/J, stock #
526 008374) mice were obtained from the Jackson Laboratory. P14 (B6;D2-
527 Tg(TcrLCMV)327Sdz/JDvs/J) mice were a generous gift from Alfred Singer (NCI, NIH). Dapl1^{ZsG}
528 mice were generated in the University of Massachusetts Animal Models core facility (see below).
529 P14^{+}Lin28Tg and P14^{+}let-7Tg mice on a *Rag2*$^{-/-}$ background were generated as previously
530 described [92]. Animals were housed in a specific pathogen-free facility under a 12-h dark/12-h light
531 cycle at 20–22 °C and a humidity range of 30–70%. All breedings were maintained at the
532 University of Massachusetts, Amherst.

533 Generation of Dapl1^{ZsG} mice

534 Dapl1^{ZsG} knock-in mice were generated in the University of Massachusetts Animal Models core
535 facility using CRISPR/Cas9-mediated genome editing. The knock-in template construct was
536 designed to replace the Stop codon of the *Dapl1* gene and contained a GSG-P2A-ZsGreen
537 fragment flanked by 120bp 5' and 3' homology arms. Two single guide RNAs (sgRNA) were used
538 to target PAM (AGG) 10 bp upstream (antisense sgRNA1: GTCCTGGTCTAACATTTTCG) and
539 PAM (AGG) 3 bp downstream (sense sgRNA2: AACCTCGAAAATGTTAGACC) of Stop codon of
540 the *Dapl1* gene, such that the original target sequence is disrupted after insertion of the construct
541 and therefore is no longer subject to Cas9 re-cutting. Single-strand DNA template (GenScript,
542 Inc), Cas9 protein, and sgRNAs (IDT, Inc) were microinjected into zygotes isolated from

543 superovulated B6D2F1 (C57BL/6J × DBA2J) female mice (8–10 weeks old) mated with B6D2F1
544 males, followed by euthanasia 20 h post-hCG injection for zygote collection from the oviducts.
545 Microinjected zygotes were cultured in KSOM medium (EMD Millipore) at 37°C in a humidified
546 atmosphere of 5% CO_2/5% O_2 balanced with N_2. After 3 days of in vitro culture, early blastocysts
547 (E3.5) were transferred into the recipients (E2.5) by using Nonsurgical Embryo Transfer
548 (ParaTechs Corporation, #60010) to produce founder mice. Correctly targeted mice (identified by
549 PCR using the primers for 5' end Dapl1F GTAGAGACTGCGACTTGACC/ZsGreenR
550 CTTCATGGTCATCTCCTTGG and for 3' end ZsGreenF TCCTGCGAGAAGATCATCC/Dapl1R
551 GAAAAGGGAAGATACAAAAGTTGG, and confirmed by sequencing) were backcrossed to
552 C57BL/6J mice for 10 generations.

553 Generation of anti-Dapl1 antibodies

554 Anti-Dapl1 antibodies were generated as described previously [93]. Briefly, recombinant Dapl1
555 protein was cloned and expressed using Novagen pET Expression System (EMD Millipore)
556 according to manufacturer's instructions. 8-week-old BalbC/J mice were immunized
557 intraperitoneally with 100 µg of the purified Dapl1 protein mixed in with Freund's adjuvant. Spleens
558 were harvested after two boosts and splenocytes were fused with SP20 myeloma cells (ATCC)
559 using electrofusion (BTX, Harward apparatus). Hyrbidomas were cultured in RPMI supplemented
560 with 20% fetal bovine serum, 100 U/mL penicillin, 0.1 mg/mL streptomycin, 2 mM L-glutamine, 1
561 mM sodium pyruvate and HAT (0.1 mM sodium hypoxanthine, 0.4 µM aminopterin, 16 µM
562 thymidine). Antibody clones were tested by ELISA on Dapl1 recombinant protein and
563 immunofluorescence on NIH-3T3 cells transduced with a Dapl1 overexpression retrovirus.

564 Flow cytometry analysis

565 Flow cytometry data were acquired on BD LSR Fortessa or Cytek™ AURORA and analyzed in
566 FlowJo™ v10.9.0 Software. The following monoclonal antibodies from BioLegend were used:
567 CD8α (53-6.7), CD8β (YTS156.7.7), CD4 (RM4-5), CD44 (IM7), CD62L (MEL-14), KLRG1
568 (2F1/KLRG1), CD127 (A7R34), PD1 (29F.1A12), Tim-3 (RMT3-23), 2B4 (m2B4(B6)458.1),

569 CD45.2 (104), CD122 (TM-β1), CD5 (53-7.3), TCRβ (H57-597), TCRγ/δ (GL3), CD11b (M1/70),
570 Ly6C (HK1.4), Ly6G (1A8), CD3 (145-2C11), NK1.1 (PK136), B220 (RA3-6B2), F480 (BM8),
571 SiglecH (551), CD11c (N418), CD24 (M1/69), CD172 (P84), CXCR3 (CXCR3-173), CD103 (2E7),
572 Ly108 (330-AJ), TNFα (MP6-XT22) and Streptavidin - AF647, PE, BV711. CD160 (CNX46-3),
573 MHCII (M5/114.15.2) and IFNγ (XMG 1.2) were from eBioscience. CD45 (30-F11) was from
574 Invitrogen. PE-CF594 rat anti-mouse IgG was from BD Biosciences. PE-conjugated CD1d
575 tetramers were obtained from the Tetramer Core Facility of the US National Institutes of Health.
576 Live cells were incubated with anti-CD16/32 Fc block (2.4G2, BD Pharmingen) prior to staining
577 with antibodies against surface markers. Staining for surface proteins was performed at 4 °C for
578 40 min, and FACS buffer (PBS + 0.5% BSA + 0.01% sodium azide) was used for washes. Dead
579 cells were stained with DAPI.
580 For intracellular cytokine staining, cell suspensions were restimulated *in vitro* for a total of 4 hours
581 with 50 ng/mL phorbol 12-myristate 13-acetate (PMA, Sigma) and 1 μM Ionomycin (Sigma), in
582 the presence of 2 μM monensin (eBioscience). After surface antibody staining, cells were stained
583 with the LIVE/DEAD fixable Blue Dead Cell Stain Kit (Thermo Fisher Scientific) according to the
584 manufacturer's instructions. Cells were then fixed and permeabilized using the Cytofix/Cytoperm
585 solution kit (BD Biosciences) according to the manufacturer's instructions, followed by staining
586 with antibodies against intracellular molecules, including Dapl1.
587 Data from Cytek™ AURORA were gated on live CD45+ TCRβ+ cells (fig. 1G, 3A) or total live
588 CD45+ cells (fig. 2E) and exported to csv files as channel values with all compensated
589 parameters. The exported data were analyzed by the Seurat package [94] using R software version
590 4.2.1. Data were loaded as count matrices and converted to a Seurat object using the
591 CreateSeuratObject() function. Fluorescence intensity representing Dapl1 or ZsGreen expression
592 was added to the metadata and included (fig. 1G, 3A) or excluded (fig. 2E) as a variable for
593 clustering. Data were normalized, scaled, and all features were used for PCA and UMAP

594 analyses. Clusters were annotated based on the fluorescence level of cell type markers. Cells
595 representing CD4+ or CD8+ cells were subset and re-clustered (fig. 1G, 3A).

596 Cell isolation

597 Lymph nodes, spleens and thymuses were gently tweezed to isolate lymphocytes. ACK lysing
598 buffer (KD Medical) was used to remove red blood cells from spleen suspensions. For purification
599 of CD8 or CD4 T cells, lymphocyte suspensions were incubated with anti-mouse CD4 (GK1.5) or
600 anti-mouse CD8 (2.43) antibodies, respectively, followed by incubation with anti-rat IgG magnetic
601 beads (BioMag, Qiagen).

602 For the isolation of IELs and LPLs, the small intestine and colon were first removed from the rest
603 of the gastrointestinal tract, onto collection media (RPMI supplemented with 25mM HEPES, 1%
604 L-glutamine, 1% penicillin/streptomycin, 50μM β-mercaptoethanol, and 3% FBS). Peyer's
605 patches lining the small intestine were removed. Tissues were cleaned by flushing out feces with
606 collection media and rinsing in PBS. Tissue fragments were agitated at 37°C for 20 minutes in
607 collection media containing 5mM EDTA and 1mM DTT, then further shaken in serum-free
608 collection media containing 2mM EDTA. The suspension was washed several times in collection
609 media and passed through a 70μm filter. For LPLs, tissue fragments were minced and agitated at
610 37°C for 25 minutes in serum-free collection media containing 1mg/mL Collagenase D and
611 0.5mg/mL DNAse. The suspension was passed through a 70μm filter, washed in collection media,
612 then purified by a 30% Percoll gradient. Finally, IELs and LPLs were resuspended in collection
613 media containing 10% FBS.

614 For TIL isolation, mice were injected subcutaneously in the right flank with 2.5 x 10^5 tumor cells.
615 On day 8, mice were intravenously injected with CD45.2-BV785 antibodies (3 mg per mouse).
616 Tumors were collected 3 minutes post-injection. They were then minced and passed through a
617 40-micron filter, spun at 1250 rpm for 5 min, and resuspended in FACS buffer.

618 For isolation of liver lymphocytes, livers of mice were perfused with 10mL PBS, followed by
619 collection and manual disassociation of tissues via filtration through a 40-micron filter. Cells were

620 then spun at 1250 rpm for 5 minutes, followed by resuspension in 5mL 37% Percoll at room
621 temperature. Resuspended cells were separated by a 20-minute room temperature spin at 800G.
622 The uppermost layers of fluid were carefully aspirated to preserve the lymphocyte pellet, which
623 was then stained for flow cytometry.

624 *In vitro* culture

625 All cultures were kept in 37°C and 7% CO_2 atmosphere in a humidified incubator. For CTL
626 generation, CD8 T cells were stimulated with irradiated splenocytes and soluble anti-CD3 mAbs
627 (1 µg/mL). Cells were cultured in RPMI supplemented with 10% fetal bovine serum, 1% HEPES,
628 1% sodium pyruvate, 1% penicillin/ streptomycin, 1% L-glutamine, 1% non-essential amino acids
629 and 0.3% β-mercaptoethanol. 48h after activation, IL-2 was added to culture media (100 U/mL)
630 and cells were differentiated for an additional 3 days. For CTL differentiation with inhibitors,
631 rapamycin (Sigma-Aldrich) was used at the final concentration of 0.5µM for the first 48 hours of
632 culture. For 24-hour activations, T cells were stimulated with plate-bound anti-CD3 mAbs (1
633 µg/mL) and anti-CD28 mAbs (5 µg/mL).

634 NIH-3T3, MC38 and Jurkat cells were obtained from ATCC. B16-GP33 [15] and NIH-3T3 cells were
635 cultured in DMEM supplemented with 10% FBS. Jurkat and MC38 cells were cultured in RPMI
636 supplemented with 10% FBS.

637 *In vivo* tumor experiments

638 After receiving a sublethal dose of irradiation (500 Rad), mice were injected subcutaneously in
639 the right flank with 2.5 x 10^5 MC38 cells. For studies involving adoptive T cell transfer, irradiated
640 mice were injected intravenously with 5 x 10^4 $P14^+$ memory cells [95], followed by subcutaneous
641 injection of 2.5 x 10^5 B16-GP33 cells the next day. Tumors were measured every 2-3 days with a
642 caliper and tumor volume was determined using the following formula: ½ x D x d^2 where D is the
643 length and d is the width. Mice were euthanized when tumors reached 2 cm^3, when tumors
644 became ulcerated, or in instances when tumors interfered with normal behavior.

645 Confocal Microscopy

646 For microscopy, iBiTreat dishes (u-slide 8 well, 80826-90) were coated with 5μg/mL fibronectin
647 overnight, then washed before seeding $1x10^4$ NIH-3T3 cells per cell. NIH-3T3 cells were imaged
648 one day after seeding the iBiTreat dishes. Cultures were rinsed with PBS, then fixed with 3.7%
649 formaldehyde at room temperature for 25 minutes. After rinsing three times with PBS, cells were
650 permeabilized with 0.5% Triton at room temperature for 5 minutes. Cells were blocked with PBS
651 containing 1% BSA for 1 hour at room temperature. Cells were stained as described in "Flow
652 cytometry analysis", using PBS + 1% BSA for washes. For naïve P14 T cells, cells in suspension
653 were stained, fixed, and permeabilized as described above. Stained cells were mixed with
654 ProLong Gold (Thermo Fisher Scientific, P36934), and sealed onto a glass slide with a coverslip.
655 Images were taken with a Nikon Eclipse Ti Series inverted microscope with a C2 confocal
656 attachment, using the Immersion oil type F (Nikon) objective for the 100x lens. Analyses were
657 performed using the Nikon Elements Analysis 3.1 software.

658 Experiments with *Listeria Monocytogenes* (LM)

659 Recombinant LM expressing GP(33-41) epitope was a gift from Dr. Harty (University of Iowa). A
660 frozen aliquot of LM (stored at −80 °C) was thawed, cultured in Tryptic Soy Broth media (KD
661 Medical) with 50 μg/mL streptomycin, and optical density at 600 nm wavelength (OD600) was
662 measured hourly. OD600 of 1 corresponds to 1 x 10^9 CFU of LM. Once OD600 reached 0.08-
663 0.09, cells were spun down for 15 min at 6000 RPM, 4°C and resuspended in 0.9% NaCl at the
664 concentration of 6 x 10^7 CFU/mL. Each recipient mouse was infected intravenously (i.v.) with 6 x
665 10^6 CFU of LM. Prior to infection but during the same day, mice were injected i.v. with 2 x 10^4
666 naïve $P14^+$ CD8 T cells.

667 Western blot analysis

668 Cells were collected and lysed in M2 lysis buffer (20mM Tris, pH7.0, 0.5% NP40, 250mM NaCl,
669 3mM EDTA, 3mM EGTA, 2mM DTT, 0.5mM PMSF, 20mM β-glycerol phosphate, 1mM sodium
670 vanadate, 1μg/mL Leupeptin), then resolved by SDS-PAGE. Blots were probed with anti-Dapl1,
671 anti-Zap70 (BD Biosciences), anti-HA (Cell Signaling) and anti-α-Tubulin (Sigma), and visualized

672 using enhanced chemiluminescence (ThermoScientific) with horse-radish peroxidase conjugated
673 anti-mouse IgG (Calbiochem) or anti-rabbit IgG (Jackson Immunoresearch).

674 Cloning, retroviral vectors and transduction

675 Open reading frames (ORF) of transcription factors (ID2, ID3, Klf2) and Dapl1 were PCR-
676 amplified using Phusion High-Fidelity DNA Polymerase (NEB) and ORF clones as templates
677 (Horizon Discoveries). The rest of transcription factors (Bcl11b, Foxo1, Bach2, Tcf7, Lef1, Klf2)
678 and HA-tagged Dapl1 constructs were synthesized (GenScript). Inserts were then cloned into
679 pMRX-IRES-GFP vector using NEBuilder HiFi DNA Assembly kit (NEB). Retroviruses were
680 produced from the transfection of Platinum-E cells with empty and gene-of-interest-expressing
681 pMRX-IRES-GFP vectors using the Transporter 5 transfection reagent (Polysciences) according
682 to the manufacturer's instructions. Viral supernatants were collected 24 hours after transfection,
683 concentrated with PEG-it (System Biosciences) and flash frozen in aliquots in liquid nitrogen. For
684 retroviral transduction of T cells, naïve lymphocytes were stimulated with irradiated splenocytes
685 in the presence of anti-CD3 mAbs (2 µg/mL) and irradiated splenocytes for 14 hours and then
686 spinfected (2000 RPM, 90 minutes, 37°C) with virus and polybrene (4 µg/mL). Media was
687 changed 4 hours after transduction, after which IL-2 was added at 100 U/mL daily until day 5 post
688 plating to generate CTLs. Jurkat cells were spinfected with virus and polybrene at 2000 RPM, 90
689 minutes, 37°C; NIH-3T3 cells were spinfected at 900 RPM, 90 minutes, 37°C.

690 Thymic egress inhibition experiments

691 Age and sex matched female Dapl1$^{ZsG/WT}$ mice were injected with 1mg/kg of the thymic egress
692 inhibitor FTY720 (Millipore Sigma) or with a 10% ethanol in PBS vehicle control intraperitoneally
693 every 48 hours for 8 days. Mice were sacrificed at day 9, and lymph nodes and spleens were
694 collected.

695 Isolation of RNA and quantitative PCR

696 RNA was isolated using The *Monarch* Total *RNA* Miniprep Kit (NEB). cDNA was synthesized
697 using the SensiFast cDNA Synthesis Kit (Thomas Scientific). SYBR Green quantitative PCR was

698 performed using the SensiFAST SYBR Lo-Rox kit (Thomas Scientific). SYBR Green primers
699 (Integrated DNA Technologies) used are as follows: Dapl1-F: ATGGCAAACGAAGTACAAGTTCT,
700 Dapl1-R: TCTTTCCAAAACGCCCATCTC, Rpl13A-F: CGAGGCATGCTGCCCCACAA, Rpl13A-
701 R: AGCAGGGACCACCATCCGCT.

702 Analysis of public RNAseq datasets

703 For reanalysis of bulk RNA sequencing data comparing Dapl1 expression in Bcl11b knockout
704 MPECs, normalized counts from GSE186283 were compared via an ordinary one-way ANOVA.
705 Graphs were generated via Graphpad Prism 10. For reanalysis of sorted thymic precursor data
706 (fig 6C), raw counts were obtained from GSE148973 [85]. Using the DESeq2 [96] package in R,
707 normalized counts and differential expression were calculated.

708 Analysis of public scRNAseq datasets

709 Single cell RNAseq Datasets were first screened for those that included clusters with a sufficient
710 amount of cells expressing *Dapl1* for calculating statistics. First, read count matrices were
711 downloaded from NCBI GEO, then analyzed using the Seurat package in R with standard
712 procedures, or with version 5.0 integration methods when appropriate. Next, cell clusters were
713 annotated based on the expression level of marker genes suggested by the original publications.
714 Finally, within respective clusters, differential gene expression was calculated between cells
715 expressing *Dapl1* at a level greater than 0.1 and cells expressing *Dapl1* at a level less than 0.1,
716 using the FindMarkers() function and the test="wilcox" option. For the meta-analysis of each cell
717 type of interest (naïve cells, Memory cells from acute infection, stem-like cells from TILs), the list
718 of differentially expressed genes were compared across different datasets and filtered for those
719 that were commonly upregulated or commonly downregulated in at least two datasets. The
720 intensity of differential expression of these genes were represented by plotting the average Log2
721 fold change values with the pheatmap package in R. Prediction of differentially enriched pathways
722 based on these genes were performed with Metascape [97], and the results were plotted using
723 ggplot2 package in R.

Datasets used for naïve cells: GSE131847 [71], GSE199563 [69], GSE213470 [72], GSE221969 [73], GSE181784 [68], GSE186839 [70].

Datasets used for memory cells from acute infection models: GSE152841 [77], GSE131847 [71], GSE182275 [76], GSE181784 [68], GSE119940 [62], GSE186839 [70].

Datasets used for Stem-like cells from tumors: E-MTAB-13073 [50], GSE180094 [6], GSE122712 [11], GSE182509 [80], GSE221118 [82], GSE217038 [81].

For the multimodal thymic CITEseq dataset GSE186078 [86], the h5ad files were downloaded and converted to a Seurat object in R. The FeaturePlot() function was used to visualize the expression of select markers and differentiation pseudotime.

Statistical analysis

Data statistical analysis was performed with Prism 10 (GraphPad software). *P*-values for comparisons of only two groups were determined using paired or unpaired two-tailed Student's *t*-tests, with Mann-Whitney corrections if normal distributions could not be assumed. Ordinary Brown-Forsythe and Welsh one-way ANOVAs comparisons were used to compare multiple conditions, and two-way ANOVAs were used to compare tumor growth curves, cell population proportions over time, and thymic egress inhibition experiments. Mixed effects analyses were used to compare multiple groups of independently normalized data. Survival comparisons were conducted using Kaplan-Meier tests. Sample size was not predetermined by statistical methods. Two mice were excluded from analysis of day 30+ data from figure 5B due to signs of secondary infection or malocclusion in adoptive transfer recipients; exclusion of these data points does not impact the interpretation of results.

Main Figures

Figure 1. Dapl1 expression is restricted to specific T cell populations. (A) Normalized *Dapl1* reads (FPKM) from RNAseq of WT (grey), Let7KD (red), and Let7Tg (blue) CTLs (GSE232541). **(B)** Dapl1 expression (normalized by DESeq2) mined from the ImmGen genome browser in TCRαβ T cell subsets. **(C)** Dapl1 protein expression (Western blot) in total thymocytes, or CD4 or CD8 T cells from peripheral lymph nodes. **(D)** Confocal microscopy of CD8 T cells stained for Dapl1 (red), CD8α (green), and DAPI (blue). **(E)** Representative flow cytometry plots of lymphocytes taken from peripheral lymph nodes of B6 mice and intracellularly stained for Dapl1. **(F)** Dapl1 expression by proportion (top) or MFI (bottom) in CD4 T cells (light blue), CD8 T cells (blue), or $CD4^-CD8^-$ (DN, grey) cells from blood (n=6), spleen (n=3), or lymph nodes (n=3) of B6 mice intracellularly stained for Dapl1. **(G)** UMAP projection of multicolor flow cytometry data from splenic T cells of B6 mice. Splenocyte populations are marked as CD4+Dapl1- (light grey), CD4+Dapl1+ (light blue), CD8+Dapl1- (dark grey), and CD8+Dapl1+ (dark blue) T cells (n=3 per group). **(H)** Flow cytometry analysis of Dapl1-positive or Dapl1-negative splenocytes using CD122 and CD44 as markers of differentiation (left), and summary statistics of underlying splenocyte populations (right). **(I)** Surface protein expression on naïve ($CD44^-CD62L^+$) T cells calculated either as the proportion of Ly6C positive cells or MFI relative to the Dapl1- population (CD5, CD44, CD62L, CD127, CD122). Statistical analyses were calculated using either an ordinary one-way ANOVA using Tukey's correction **(A, F top)**, two-tailed unpaired *t*-tests **(F bottom)**, or two-tailed paired *t*-tests **(G, I)**. All data are representative of three biological replicates from one RNA-seq analysis **(A)**, two or more independent experiments **(B-G)**, or are pooled from three biological replicates from two independent experiments **(E-I)**.

Figure 2. Characterization of Dapl1 reporter. (A) CRISPR-Cas9 mediated $Dapl1^{ZsG}$ reporter gene construct strategy, representing introduction of P2A-ZsGreen to the end of Exon 4. **(B)** Representative flow cytometry plot of lymphocytes from peripheral lymph nodes of $Dapl1^{ZsG/WT}$ mice (n=3, left). Data are summarized by proportion or MFI in CD4 T cells (light green), CD8 T cells (green), or $CD4^-CD8^-$ (DN, grey) cells (right). **(C)** Western blot analysis of Dapl1 and Zap70 expression in whole cell lysates from CD8 T cells enriched from lymph nodes of WT, $Dapl1^{ZsG/WT}$, or $Dapl1^{ZsG/ZsG}$ mice. **(D)** Representative UMAP projection (left) of multicolor flow cytometry data from spleen of $Dapl1^{ZsG/WT}$ mice clustered via Seurat. ZsGreen fluorescence is represented as both a featureplot (middle) or violin plots split by cell subset (right). **(E)** Representative flow cytometry plots of splenocytes from $Dapl1^{ZsG/WT}FoxP3^{RFP/RFP}$ mice. **(F-K)** Proportion of ZsGreen expressing cells within **(F)** spleen, **(G)** liver and **(H)** gut subsets: small intestine intraepithelial lymphocyte (IEL), small intestine lamina propria lymphocyte (LPL), colon IEL, or colon LPL. All statistical analyses were calculated using ordinary one-way ANOVAs with Tukey's correction for multiple comparisons. All data are representative of more than three independent experiments **(B,E,F)**, one experiment **(C-D)**, three biological replicates from one experiment **(G)**, or at least two biological replicates pooled from three independent experiments **(H-K)**.

Figure 3. Dapl1 expression marks distinct subpopulation of naïve CD8 T cells (A) Representative UMAP projection of multicolor flow cytometry data from splenic T cells of $Dapl1^{ZsG/WT}Foxp3^{RFP/RFP}$ mice clustered via Seurat. Splenocyte populations are marked as CD4+ZsG- (light grey), CD4+ZsG+ (light green), CD8+ZsG- (grey), CD8+ZsG+ (dark green), ZsG-Tregs (dark grey), and ZsG+Tregs (red). **(B)** Flow cytometric analysis of ZsGreen-positive or ZsGreen-negative splenocytes using CD122 and CD44 as markers of differentiation (left), and summary statistics of underlying splenocyte populations (right). **(C)** Summary statistics of

individual surface marker expression on naïve ($CD44^{low}CD62L^{high}$) T cells, calculated either as the proportion of Ly6C-positive cells or MFI relative to the ZsGreen- population (CD5, CD44, CD62L, CD127). **(D)** Representative flow cytometry plots demonstrating heterogeneity of Dapl1 expression among circulating WT $Dapl1^{ZsG/WT}$, $Dapl1^{ZsG/WT}P14^{+}Rag2^{-/-}$, or $Dapl1^{ZsG/WT}OTI^{+}Rag2^{-/-}$ CD8 T cells. **(E)** ScRNAseq analysis of naïve CD8 T cells from $P14^{+}Rag2^{-/-}$, $OTI^{+}Rag2^{-/-}$, or WT datasets (GSE131847, GSE199563, GSE213470, GSE221969, GSE181784, GSE186839), consisting of (top) violin plots representing Dapl1 heterogeneity, (middle) descriptions of the datasets, and (bottom) a heatmap of consistently differentially expressed genes among datasets. **(F)** Pathway enrichment analysis denoting significantly different pathways between Dapl1 positive and Dapl1 negative naïve CD8 T cells. Statistical analysis for **(B, C)** was calculated via two-tailed paired *t* tests for difference. All data are pooled from three biological replicates from at least two independent experiments **(A-C)**, or representative of at least three independent experiments **(D)**.

Figure 4. Biased differentiation of Dapl1+ CD8 T cells. (A) Schematic of $P14^{+}Rag2^{-/-}$ CD8 T cell differentiation into CTLs (top left). Representative flow cytometry plots of Dapl1 expression in CTLs (bottom left). Proportions of $CD62L^{+}Tim3^{-}$ or $CD62L^{-}Tim3^{+}$ cells in Dapl1- and Dapl1+ populations (bottom middle) and MFI fold change of surface markers relative to Dapl1- cells (n = 3, bottom right). **(B)** ZsGreen expression in CTLs from $Dapl1^{ZsG/WT}P14^{+}Rag2^{-/-}$ reporter mice (left). Proportions of $CD62L^{+}Tim3^{-}$ or $CD62L^{-}Tim3^{+}$ cells in $ZsGreen^{-}$ and $ZsGreen^{+}$ populations (middle) and MFI fold changes of surface markers relative to $ZsGreen^{-}$ cells (n = 2, right). **(C)** Proportions of $ZsGreen^{+}$ CTLs when differentiated with DMSO or rapamycin-supplemented media for the first 48h of activation (n = 3). **(D)** Schematic of LM-GP33 challenge and adoptive T cell transfer (top). Flow cytometry plots of ZsGreen expression at days 0, 7, 14 (blood), and 30+ (spleen) post-infection (n = 8, left). Temporal changes in population proportions over time: $ZsGreen^{-}$ sorted cells which continued to be $ZsGreen^{-}$ (ZsG-, grey), $ZsGreen^{+}$ cells within the $ZsGreen^{-}$ sorted group (*De novo*, black), sorted cells which lost ZsGreen expression (Ex-ZsG, purple), and cells which retained ZsGreen (ZsG+, green, right). **(E)** Surface expression of KLRG1 vs CD127 and CD62L vs CD44 on CD8 T cells at days 7, 14 (blood), and 30+ (spleen) (left). Frequencies of SLECs, INT, MPECs, effector memory, and central memory populations within ZsG-, Ex- ZsG, and ZsG+ groups (n = 8, right). **(F)** Analysis of publicly available scRNAseq datasets of memory CD8 T cells generated via LCMV Armstrong (Arm) (GSE152841, GSE131847, GSE182275, GSE181784, GSE119940) or influenza A virus (IAV) (GSE186839), consisting of (top) violin plots representing *Dapl1* heterogeneity, (middle) descriptions of the datasets, and (bottom) a heatmap of consistently differentially expressed genes among datasets. **(G)** Proportions of Dapl1+, $CD62L^{+}Tim3^{-}$, or $CD62L^{-}Tim3^{+}$ CTLs by intracellular staining following transcription factor overexpression with GFP-tagged vectors, presented as fold change in GFP+ vs. GFP− cells (n = 3). Statistical analysis was calculated using two-tailed paired *t*-tests **(A, B),** a two-tailed unpaired *t*-test **(C)**, ordinary two-way ANOVA with FDR correction **(D)**, ordinary one-way ANOVAs using Tukey's correction **(E),** or ordinary one-way ANOVAs using Dunnet's correction **(G)**. Data are representative of two or more independent experiments (**A-D**) or are pooled from three independent experiments (**G**).

Figure 5. Role of Dapl1 expression in differentiation of CD8 T cells. (A) Experimental design of LM-GP33 challenge and adoptive T cell transfer (top). Representative flow cytometry plots of Dapl1 or ZsGreen expression in adoptively transferred $P14^{+}Rag2^{-/-}$ or $Dapl1^{ZsG/ZsG}P14^{+}Rag2^{-/-}$ CD8 T cells at days 0, 7, or 14 post-infection in the blood and day 30+ in the spleen (left), with dynamic changes in proportions of WT Dapl1+ (blue) or Dapl1-wannabe (peach) cells over time (right). **(B)** Representative flow cytometry plots of the surface expression of KLRG1 vs CD127 (Day 7, 14) and CD62L vs CD44 (Day 30+) on CD8 T cells at day 7 and 14 post-infection in the

blood and day 30 in the spleen (left). Quantification of the frequencies of SLECs, INT, MPECs, effector memory, and central memory populations within Dapl1-negative, Dapl1-positive, ZsGreen-negative, and Dapl1-wannabe populations (right). **(C)** Representative flow cytometry plots of TNFα and IFNγ secretion of day 30+ memory CD8 T cells 4 hours post stimulation with ionomycin and PMA (left), with quantification (right). All summary plots are pooled from 12 (WT) and 13 (Dapl1$^{ZsG/ZsG}$) biological replicates at days 7 and 14, and 8 biological replicates at day 30+ for both groups from three independent experiments **(A-B)**, or 8 (WT) or 6 (Dapl1$^{ZsG/ZsG}$) biological replicates pooled from two independent experiments **(C)**. Statistical analyses were conducted via ordinary two-way ANOVA with FDR correction **(A)**, Brown-Forsythe and Welsh ANOVA tests **(B),** or a mixed-effects analysis with Šidák's correction **(C)**.

Figure 6. Dapl1+ naïve T cells originate from mature thymocytes. (A) Flow cytometry plots of FoxP3 and ZsGreen expression on splenocytes from one- day (n = 4), one-week (n = 4), or one-month (n =3) old Dapl1$^{ZsG/WT}$FoxP3$^{RFP/RFP}$ mice (left), with quantification of ZsGreen expression among CD4 (light green), CD8 (dark green), and Treg (red) subsets (right). **(B)** Expression of ZsGreen in Dapl1$^{ZsG/WT}$ mice on mature thymic CD4 and CD8 populations, as marked by TCRβ (left), with summary (right). **(C)** *Dapl1* expression by RNAseq of thymic subsets sorted by maturity from (top, GSE148973), with heatmaps of defining characteristics by subset (bottom). **(D)** UMAP plots regenerated from a single-cell multimodal thymocyte dataset (GSE186078) denoting pseudotime, *Cd4*, *Cd8*, and *Dapl1* expression. **(E)** Flow cytometry histogram of surface CD24 expression in CD8α$^+$ cells from the thymus or lymph nodes of Dapl1$^{ZsG/WT}$ mice stratified by ZsGreen expression (left), with summary (right). **(F)** ZsGreen MFI in CD8α$^+$ cells from the thymus or lymph nodes of Dapl1$^{ZsG/WT}$ mice (n=3). **(G)** Flow cytometry plots denoting ZsGreen expression in thymocytes from Dapl1$^{ZsG/WT}$ mice treated with daily intraperitoneal injections of either ethanol (n=2) or FTY720 (n=3), with summary of replicates (right). All data are representative of two to four biological replicates from one experiment **(A,G)**, or are representative of at least two independent experiments **(B,E,F)**. Statistical analysis was conducted using either an ordinary two-way ANOVAs using Tukey's correction **(A,G)**, matched one-way Anova with Geisser-Greenhouse correction **(B)**, DESEQ2 **(C)**, one-way Welsh's Anova **(E)**, or two-tailed unpaired *t* test **(F)**.

Supplementary Figures

Figure S1. (A) ELISA verification of anti-Dapl1 clone 6H9 monoclonal antibodies (n=8 per group). Each dot represents a well of a 96-well plate. **(B)** Protein expression (Western blot) of Dapl1 in 3T3 cells transduced with either an empty-pMRX or Dapl1-pMRX virus, using anti-Dapl1 clone 6H9 antibodies. **(C)** Confocal microscopy of 3T3 cells transduced with either an empty-pMRX or Dapl1-pMRX virus and stained for Dapl1. Dapl1 staining is shown with red, GFP with green, and DAPI with blue. **(D)** Violin plots of underlying expression patterns of all protein markers in splenocytes used for clustering in figure 1G. **(E)** Gating schema and expression patterns of CD62L and CD44 used for figure 1H to define naïve and differentiated T cells. **(F)** Representative histograms of surface marker expression on naïve splenocytes used to generate Figure 1I summary plots. Data are either pooled from three independent experiments **(A)**, from a single experiment **(B)**, or representative of at least two independent experiments **(C-F)**. Statistical analysis for **(A)** was calculated using a two-tailed unpaired *t* test.

Figure S2. (A). Initial population proportions and post-sort purity of ZsGreen- or ZsGreen+ CD8 T cells collected from lymph nodes of Dapl1$^{ZsG/ZsG}$ mice and sorted by ZsGreen expression (left), followed by expression of Dapl1 mRNA as detected by qPCR (right). **(B)** Protein expression of Dapl1 (Western blot) in untransduced Jurkat cells, Jurkat cells overexpressing modified N-terminus HA tagged Dapl1 (HA-Dapl1), or Jurkat cells overexpressing modified C-terminus HA tagged Dapl1 (Dapl1-HA). **(C)** Violin plots of surface protein expression of all markers analyzed for the splenic immune populations characterized in Figure 2D. Data are representative of at least two independent experiments **(A)**, or one experiment **(B,C)**.

Figure S3. (A) Gating strategies and representative plots used to characterize T cell populations in the spleen of Dapl1$^{ZsG/WT}$ mice, as summarized in Fig. 2F. **(B)** Gating strategies and representative plots used to characterize T cell populations in the liver of Dapl1$^{ZsG/WT}$ mice, as summarized in Figure 2G. All data are representative of three or more biological replicates.

Figure S4. (A-D) Gating strategies and representative flow cytometry plots used to characterize T cell populations in **(A)** small intestine IELs, **(B)** small intestine LPLs, **(C)** colon IELs, or **(D)** colon LPLs of Dapl1$^{ZsG/WT}$ mice, as summarized in Figure 2 H. All data are representative of 2-3 biological replicates from three independent experiments.

Figure S5. (A) Violin plots of surface protein expression of all markers analyzed for the splenic immune populations characterized in Figure 3A. **(B)** Gating strategy and representative flow cytometry plots used to identify CD4^{+}FoxP3^{RFP-}, CD4^{+}FoxP3^{RFP+}, CD8α^{+}FoxP3^{RFP-}, CD8α^{+}FoxP3^{RFP+} T cell populations in spleens of Dapl1$^{ZsG/WT}$ FoxP3$^{RFP/RFP}$ mice **(C)** Representative flow cytometry histograms of surface proteins on naïve (CD44^{low}CD62L^{high}) CD4 and CD8 T cells from Dapl1$^{ZsG/WT}$ FoxP3$^{RFP/RFP}$ mice. **(D)** Representative flow cytometry histograms of surface proteins on CD4^{+}FoxP3^{RFP+} T regulatory cells from Dapl1$^{ZsG/WT}$FoxP3$^{RFP/RFP}$ mice**. (E)** Summary statistics of individual surface marker expression on CD4^{+}FoxP3^{RFP+} T regulatory cells from Dapl1$^{ZsG/WT}$FoxP3$^{RFP/RFP}$ mice, calculated either as MFI relative to the ZsGreen- population or as the proportion of ZsGreen positive or negative cells which express the indicated marker. All data are representative of three biological replicates from two independent experiments **(C)**. All statistical analysis was conducted using two-tailed paired *t* tests for difference.

Figure S6. (A-B) Representative flow cytometry histograms of surface markers on CTLs differentiated either from **(A)** WT P14^{+}Rag2$^{-/-}$ or **(B)** Dapl1$^{ZsG/WT}$P14^{+}Rag2$^{-/-}$ CD8 T cells. **(C)** Experimental design and representative surface marker expression from Dapl1$^{ZsG/WT}$P14^{+}Rag2$^{-/-}$ CD8 T cells sorted by ZsGreen expression and differentiated into CTLs. **(D)** Total number of CD8 T cells collected from spleens and lymph nodes of mice 30+ days post adoptive transfer of Dapl1$^{ZsG/WT}$P14^{+}Rag2$^{-/-}$ CD8 T cells sorted by ZsGreen expression, followed by LM-GP33 challenge (n=8 per group). **(E)** CD62L surface expression on sorted CD8 T cells at day 7 and 14 post-infection in the blood and day 30^{+} in the spleen (n=8 per group). **(F)** ScRNAseq clustering of memory CD8 T cell subsets from GSE181784, with *Dapl1* expression marked in blue (right). **(G)** Pathways enriched by genes upregulated (orange) or downregulated (blue) in *Dapl1*$^{+}$ memory CD8 T cells generated via LCMV Armstrong (Arm) (GSE152841, GSE131847, GSE182275, GSE181784, GSE119940) or influenza A virus (IAV) (GSE186839). All data are representative of three biological replicates (**A**), two biological replicates (**B**), three independent experiments (**C**), or two independent experiments (**D-E**). Statistical analyses were conducted using an unpaired two-tailed *t* test (**D**), or an ordinary one-way Anova with Tukey's correction (**E**).

Figure S7. (A) Proposed model of naïve T cell differentiation, where a subset of Dapl1+ cells (marked in red) is maintained exclusively in the memory lineage.

Figure S8. **(A)** Representative flow cytometry plots of P14^{+}Rag2$^{-/-}$ CD8 T cells transduced with GFP-reported transcription factor overexpression vectors, demonstrating transduction efficiency (left), and Dapl1 (middle) or Tim3, and CD62L protein levels (right) stratified by GFP expression. **(B)** Bulk RNAseq analysis of sorted CD8 T cell MPECs (KLRG1^{-}CD127^{+}) or SLECs (KLRG1^{+}CD127^{-}) day 9 post LM-OVA challenge from either Bcl11b$^{-/-}$ or WT mice (GSE186283). Data are representative of three independent experiments **(A)**, or one bulk RNA sequencing dataset with three biological replicates (**B**).

Figure S9. (A) Schema of tumor infiltrating lymphocyte (TIL) experiment (top), with Tim3 and CD62L surface expression on Dapl1- or Dapl1+ TILs at day 8 post B16 melanoma implantation into WT mice (bottom). CD45.2 was injected into mice before sacrifice to exclude circulating cells in analysis (n=6 tumors). **(B)** Representative histograms denoting CD44 surface expression on tumor draining lymph nodes (TDLNs), TILs, and CD45.2^{+} contamination of day 8 WT TILs intracellularly stained for Dapl1. **(C)** Experimental schema (top) and summary proportions (bottom) of CD62L^{-}Tim3^{+} and CD62L^{+}Tim3^{-} cells within ZsG+ or ZsG- TILs at day 8 post B16 melanoma implantation into Dapl1$^{ZsG/WT}$ mice, as well as Ly108 MFI normalized to the average Ly108 MFI of ZsG- cells. (**D**) scRNAseq analysis of tumor infiltrating CD8 T cells (E-MTAB-13073), indicating Dapl1 expression in Tpex and Tex subsets. **(E)** ScRNAseq analysis of tumor infiltrating CD8 T cells from publicly available datasets (E-MTAB-13073, GSE180094, GSE122712, GSE182509, GSE221118, GSE217038), consisting of (top) violin plots representing *Dapl1* heterogeneity in stem-like TILs, (middle) descriptions of the datasets, and (bottom) a heatmap of consistently differentially expressed genes among datasets. **(F)** Pathways enriched by genes upregulated (orange) or downregulated (blue) in *Dapl1*$^{+}$ stem-like TILs. Data are either pooled from two independent experiments **(A, C)**, or are from one experiment **(B)**. All statistical analysis of flow cytometry data was conducted via two-tailed unpaired *t* tests.

Figure S10. (A) CD62L surface expression on WT P14^{+}Rag2$^{-/-}$ or Dapl1$^{ZsG/ZsG}$P14^{+}Rag2$^{-/-}$ CD8 T cells at day 7 and 14 post-LM-GP33 infection in the blood and day 30^{+} in the spleen, stratified by Dapl1 or ZsGreen expression. **(B)** Schematic of Dapl1$^{ZsG/ZsG}$P14^{+}Rag2$^{-/-}$ CD8 T cell differentiation into CTLs (top). Representative flow cytometry plots of ZsG expression on day 5 CTLs (left).

Proportions of CD62L^{+}Tim3^{-} or CD62L^{-}Tim3^{+} cells in ZsG- and ZsG+ populations (right). **(C)** Experimental schema (top), representative flow cytometry plots (left), and summary proportions (right) of CD62L^{-}Tim3^{+} and CD62L^{+}Tim3^{-} surface expression on ZsG+ or ZsG- TILs at day 8 post B16 melanoma implantation into Dapl1$^{ZsG/ZsG}$ mice. **(D)** Efficiency of Dapl1-mCherry and Empty-mCherry viruses on cultured CD8 T cells 24 hours after transduction (left). Proportions and phenotypes of Dapl1-mCherry and Empty-mCherry positive cells 7 days after adoptive transfer into Rag2$^{-/-}$ hosts and LM-GP33 infection (middle), with summary statistics (right). **(E)** Experimental schema of sort and adoptive transfer of memory CD8 T cells into B6 hosts 30+ days post LM-GP33 priming to treat B16-GD33 melanoma (top), with tumor growth curves (left) and survival curves (right). **(F)** Experimental schema of MC38 tumor challenge of WT, Dapl1$^{ZsG/WT}$, and Dapl1$^{ZsG/ZsG}$ hosts (top), with tumor growth curves (left) and survival curves (right). Statistical analysis was conducted using either a mixed-effect analysis **(A)**, two-tailed paired *t* tests for difference **(B)**, or two-way ANOVAs **(D-F)**. All survival analysis was conducted using Kaplan-Meier's test. Data are either pooled from three independent experiments **(A)**, pooled from four independent experiments **(B)**, or are from one experiment **(C-F)**.

Figure S11. (A) Gating strategies and representative flow cytometry plots used to characterize T cell populations in the thymus of Dapl1$^{ZsG/WT}$ mice, with summary statistics (n=3). **(B)** Flow cytometry plots denoting ZsGreen expression in T cells derived from lymph nodes of Dapl1$^{ZsG/WT}$ mice treated with daily IP injections of either ethanol (n=2) or FTY720 (n=3), with summary of replicates (right). Statistical analysis was conducted using either an ordinary one-way ANOVA (**A**) or an ordinary two-way ANOVAs using Tukey's correction (**B**).

1002 **References**

1003 1. Blackburn, S.D., Shin, H., Freeman, G.J. & Wherry, E.J. Selective expansion of a subset
1004 of exhausted CD8 T cells by alphaPD-L1 blockade. *Proc Natl Acad Sci U S A* **105**,
1005 15016-21 (2008).
1006 2. Chang, J.T., Wherry, E.J. & Goldrath, A.W. Molecular regulation of effector and memory
1007 T cell differentiation. *Nat Immunol* **15**, 1104-15 (2014).
1008 3. Gebhardt, T., Park, S.L. & Parish, I.A. Stem-like exhausted and memory CD8(+) T cells
1009 in cancer. *Nat Rev Cancer* **23**, 780-798 (2023).
1010 4. Geiger, R. *et al.* L-Arginine Modulates T Cell Metabolism and Enhances Survival and
1011 Anti-tumor Activity. *Cell* **167**, 829-842 e13 (2016).
1012 5. Huang, A.C. *et al.* T-cell invigoration to tumour burden ratio associated with anti-PD-1
1013 response. *Nature* **545**, 60-65 (2017).
1014 6. Huang, Q. *et al.* The primordial differentiation of tumor-specific memory CD8(+) T cells
1015 as bona fide responders to PD-1/PD-L1 blockade in draining lymph nodes. *Cell* **185**,
1016 4049-4066 e25 (2022).
1017 7. Im, S.J. *et al.* Defining CD8+ T cells that provide the proliferative burst after PD-1
1018 therapy. *Nature* **537**, 417-421 (2016).
1019 8. Kallies, A., Zehn, D. & Utzschneider, D.T. Precursor exhausted T cells: key to successful
1020 immunotherapy? *Nat Rev Immunol* **20**, 128-136 (2020).
1021 9. Krishna, S. *et al.* Stem-like CD8 T cells mediate response of adoptive cell
1022 immunotherapy against human cancer. *Science* **370**, 1328-1334 (2020).
1023 10. LaFleur, M.W. *et al.* PTPN2 regulates the generation of exhausted CD8(+) T cell
1024 subpopulations and restrains tumor immunity. *Nat Immunol* **20**, 1335-1347 (2019).
1025 11. Miller, B.C. *et al.* Subsets of exhausted CD8(+) T cells differentially mediate tumor
1026 control and respond to checkpoint blockade. *Nat Immunol* **20**, 326-336 (2019).
1027 12. Sade-Feldman, M. *et al.* Defining T Cell States Associated with Response to Checkpoint
1028 Immunotherapy in Melanoma. *Cell* **175**, 998-1013 e20 (2018).
1029 13. Siddiqui, I. *et al.* Intratumoral Tcf1(+)PD-1(+)CD8(+) T Cells with Stem-like Properties
1030 Promote Tumor Control in Response to Vaccination and Checkpoint Blockade
1031 Immunotherapy. *Immunity* **50**, 195-211 e10 (2019).
1032 14. Thommen, D.S. *et al.* A transcriptionally and functionally distinct PD-1(+) CD8(+) T cell
1033 pool with predictive potential in non-small-cell lung cancer treated with PD-1 blockade.
1034 *Nat Med* **24**, 994-1004 (2018).
1035 15. Wells, A.C. *et al.* Let-7 enhances murine anti-tumor CD8 T cell responses by promoting
1036 memory and antagonizing terminal differentiation. *Nat Commun* **14**, 5585 (2023).
1037 16. Zehn, D., Thimme, R., Lugli, E., de Almeida, G.P. & Oxenius, A. 'Stem-like' precursors
1038 are the fount to sustain persistent CD8(+) T cell responses. *Nat Immunol* **23**, 836-847
1039 (2022).
1040 17. Ahmed, R., Bevan, M.J., Reiner, S.L. & Fearon, D.T. The precursors of memory: models
1041 and controversies. *Nat Rev Immunol* **9**, 662-8 (2009).
1042 18. Akondy, R.S. *et al.* Origin and differentiation of human memory CD8 T cells after
1043 vaccination. *Nature* **552**, 362-367 (2017).
1044 19. Buchholz, V.R., Schumacher, T.N. & Busch, D.H. T Cell Fate at the Single-Cell Level.
1045 *Annu Rev Immunol* **34**, 65-92 (2016).
1046 20. Chang, J.T. *et al.* Asymmetric T lymphocyte division in the initiation of adaptive immune
1047 responses. *Science* **315**, 1687-91 (2007).
1048 21. Gerlach, C. *et al.* Heterogeneous differentiation patterns of individual CD8+ T cells.
1049 *Science* **340**, 635-9 (2013).
1050 22. Guo, A. *et al.* cBAF complex components and MYC cooperate early in CD8(+) T cell
1051 fate. *Nature* **607**, 135-141 (2022).

1052 23. Kaech, S.M. & Ahmed, R. Memory CD8+ T cell differentiation: initial antigen encounter
1053 triggers a developmental program in naive cells. *Nat Immunol* **2**, 415-22 (2001).
1054 24. Kakaradov, B. *et al.* Early transcriptional and epigenetic regulation of CD8(+) T cell
1055 differentiation revealed by single-cell RNA sequencing. *Nat Immunol* **18**, 422-432 (2017).
1056 25. Mercado, R. *et al.* Early programming of T cell populations responding to bacterial
1057 infection. *J Immunol* **165**, 6833-9 (2000).
1058 26. Stemberger, C. *et al.* A single naive CD8+ T cell precursor can develop into diverse
1059 effector and memory subsets. *Immunity* **27**, 985-97 (2007).
1060 27. Verbist, K.C. *et al.* Metabolic maintenance of cell asymmetry following division in
1061 activated T lymphocytes. *Nature* **532**, 389-93 (2016).
1062 28. Deep, D. *et al.* Precursor central memory versus effector cell fate and naive CD4+ T cell
1063 heterogeneity. *J Exp Med* **221**(2024).
1064 29. Eggert, J. & Au-Yeung, B.B. Functional heterogeneity and adaptation of naive T cells in
1065 response to tonic TCR signals. *Curr Opin Immunol* **73**, 43-49 (2021).
1066 30. Hale, B.D. *et al.* Cellular architecture shapes the naive T cell response. *Science* **384**,
1067 eadh8697 (2024).
1068 31. Ju, Y.J. *et al.* Self-reactivity controls functional diversity of naive CD8(+) T cells by co-
1069 opting tonic type I interferon. *Nat Commun* **12**, 6059 (2021).
1070 32. Li, J. *et al.* KIR(+)CD8(+) T cells suppress pathogenic T cells and are active in
1071 autoimmune diseases and COVID-19. *Science* **376**, eabi9591 (2022).
1072 33. Rogers, D. *et al.* Pre-existing chromatin accessibility and gene expression differences
1073 among naive CD4(+) T cells influence effector potential. *Cell Rep* **37**, 110064 (2021).
1074 34. Rudd, B.D. Neonatal T Cells: A Reinterpretation. *Annu Rev Immunol* **38**, 229-247
1075 (2020).
1076 35. Bartleson, J.M. *et al.* Strength of tonic T cell receptor signaling instructs T follicular
1077 helper cell-fate decisions. *Nat Immunol* **21**, 1384-1396 (2020).
1078 36. ElTanbouly, M.A. *et al.* VISTA is a checkpoint regulator for naive T cell quiescence and
1079 peripheral tolerance. *Science* **367**(2020).
1080 37. Mandl, J.N., Monteiro, J.P., Vrisekoop, N. & Germain, R.N. T cell-positive selection uses
1081 self-ligand binding strength to optimize repertoire recognition of foreign antigens.
1082 *Immunity* **38**, 263-274 (2013).
1083 38. Persaud, S.P., Parker, C.R., Lo, W.L., Weber, K.S. & Allen, P.M. Intrinsic CD4+ T cell
1084 sensitivity and response to a pathogen are set and sustained by avidity for thymic and
1085 peripheral complexes of self peptide and MHC. *Nat Immunol* **15**, 266-74 (2014).
1086 39. Weber, K.S. *et al.* Distinct CD4+ helper T cells involved in primary and secondary
1087 responses to infection. *Proc Natl Acad Sci U S A* **109**, 9511-6 (2012).
1088 40. Chen, H.B. *et al.* DAPL1 is a novel regulator of testosterone production in Leydig cells of
1089 mouse testis. *Sci Rep* **11**, 18532 (2021).
1090 41. Grassmann, F. *et al.* A Candidate Gene Association Study Identifies DAPL1 as a
1091 Female-Specific Susceptibility Locus for Age-Related Macular Degeneration (AMD).
1092 *Neuromolecular Med* **17**, 111-20 (2015).
1093 42. Hattori, Y. *et al.* Attenuation of growth hormone production at the fetal stage is critical for
1094 dioxin-induced developmental disorder in rat offspring. *Biochem Pharmacol* **186**, 114495
1095 (2021).
1096 43. Ma, X. *et al.* DAPL1 prevents epithelial-mesenchymal transition in the retinal pigment
1097 epithelium and experimental proliferative vitreoretinopathy. *Cell Death Dis* **14**, 158
1098 (2023).
1099 44. Ma, X. *et al.* DAPL1, a susceptibility locus for age-related macular degeneration, acts as
1100 a novel suppressor of cell proliferation in the retinal pigment epithelium. *Hum Mol Genet*
1101 **26**, 1612-1621 (2017).

1102 45. Zhu, L. *et al.* Dapl1 controls NFATc2 activation to regulate CD8(+) T cell exhaustion and
1103 responses in chronic infection and cancer. *Nat Cell Biol* **24**, 1165-1176 (2022).
1104 46. Leesch, F. *et al.* A molecular network of conserved factors keeps ribosomes dormant in
1105 the egg. *Nature* **613**, 712-720 (2023).
1106 47. Ma, X. *et al.* DAPL1 deficiency in mice impairs antioxidant defenses in the RPE and
1107 leads to retinal degeneration with AMD-like features. *Redox Biol* **62**, 102675 (2023).
1108 48. Baharom, F. *et al.* Intravenous nanoparticle vaccination generates stem-like TCF1(+)
1109 neoantigen-specific CD8(+) T cells. *Nat Immunol* **22**, 41-52 (2021).
1110 49. Carmona, S.J., Siddiqui, I., Bilous, M., Held, W. & Gfeller, D. Deciphering the
1111 transcriptomic landscape of tumor-infiltrating CD8 lymphocytes in B16 melanoma tumors
1112 with single-cell RNA-Seq. *Oncoimmunology* **9**, 1737369 (2020).
1113 50. Castiglioni, A. *et al.* Combined PD-L1/TGFbeta blockade allows expansion and
1114 differentiation of stem cell-like CD8 T cells in immune excluded tumors. *Nat Commun* **14**,
1115 4703 (2023).
1116 51. Chen, A.C.Y. *et al.* The aged tumor microenvironment limits T cell control of cancer. *Nat*
1117 *Immunol* **25**, 1033-1045 (2024).
1118 52. Dean, J.W. *et al.* The aryl hydrocarbon receptor cell intrinsically promotes resident
1119 memory CD8(+) T cell differentiation and function. *Cell Rep* **42**, 111963 (2023).
1120 53. Highton, A.J. *et al.* Single-cell transcriptome analysis of CD8 (+) T-cell memory inflation.
1121 *Wellcome Open Res* **4**, 78 (2019).
1122 54. Hou, S. *et al.* Virtual memory T cells orchestrate extralymphoid responses conducive to
1123 resident memory. *Sci Immunol* **6**, eabg9433 (2021).
1124 55. Lan, X. *et al.* Antitumor progenitor exhausted CD8(+) T cells are sustained by TCR
1125 engagement. *Nat Immunol* **25**, 1046-1058 (2024).
1126 56. Pauken, K.E. *et al.* Single-cell analyses identify circulating anti-tumor CD8 T cells and
1127 markers for their enrichment. *J Exp Med* **218**(2021).
1128 57. Roychoudhuri, R. *et al.* Transcriptional profiles reveal a stepwise developmental
1129 program of memory CD8(+) T cell differentiation. *Vaccine* **33**, 914-23 (2015).
1130 58. Tsui, C. *et al.* MYB orchestrates T cell exhaustion and response to checkpoint inhibition.
1131 *Nature* **609**, 354-360 (2022).
1132 59. Van Der Byl, W. *et al.* The CD8(+) T cell tolerance checkpoint triggers a distinct
1133 differentiation state defined by protein translation defects. *Immunity* **57**, 1324-1344 e8
1134 (2024).
1135 60. Vokali, E. *et al.* Lymphatic endothelial cells prime naive CD8(+) T cells into memory cells
1136 under steady-state conditions. *Nat Commun* **11**, 538 (2020).
1137 61. Yao, C. *et al.* BACH2 enforces the transcriptional and epigenetic programs of stem-like
1138 CD8(+) T cells. *Nat Immunol* **22**, 370-380 (2021).
1139 62. Yao, C. *et al.* Single-cell RNA-seq reveals TOX as a key regulator of CD8(+) T cell
1140 persistence in chronic infection. *Nat Immunol* **20**, 890-901 (2019).
1141 63. Zou, D. *et al.* CD4(+) T cell immunity is dependent on an intrinsic stem-like program. *Nat*
1142 *Immunol* **25**, 66-76 (2024).
1143 64. Heng, T.S., Painter, M.W. & Immunological Genome Project, C. The Immunological
1144 Genome Project: networks of gene expression in immune cells. *Nat Immunol* **9**, 1091-4
1145 (2008).
1146 65. Azzam, H.S. *et al.* Fine tuning of TCR signaling by CD5. *J Immunol* **166**, 5464-72
1147 (2001).
1148 66. Delpoux, A. *et al.* TCR signaling events are required for maintaining CD4 regulatory T
1149 cell numbers and suppressive capacities in the periphery. *J Immunol* **193**, 5914-23
1150 (2014).
1151 67. Lee, J.Y. *et al.* Phenotypic and Functional Changes of Peripheral Ly6C(+) T Regulatory
1152 Cells Driven by Conventional Effector T Cells. *Front Immunol* **9**, 437 (2018).

1153 68. Chen, Y., Shen, J., Kasmani, M.Y., Topchyan, P. & Cui, W. Single-Cell Transcriptomics
1154 Reveals Core Regulatory Programs That Determine the Heterogeneity of Circulating and
1155 Tissue-Resident Memory CD8(+) T Cells. *Cells* **10**(2021).
1156 69. Giles, J.R. *et al.* Shared and distinct biological circuits in effector, memory and
1157 exhausted CD8(+) T cells revealed by temporal single-cell transcriptomics and
1158 epigenetics. *Nat Immunol* **23**, 1600-1613 (2022).
1159 70. Guo, K. *et al.* The chemokine receptor CXCR3 promotes CD8(+) T cell-dependent lung
1160 pathology during influenza pathogenesis. *Sci Adv* **10**, eadj1120 (2024).
1161 71. Kurd, N.S. *et al.* Early precursors and molecular determinants of tissue-resident memory
1162 CD8(+) T lymphocytes revealed by single-cell RNA sequencing. *Sci Immunol* **5**(2020).
1163 72. Quezada, L.K. *et al.* Early transcriptional and epigenetic divergence of CD8+ T cells
1164 responding to acute versus chronic infection. *PLoS Biol* **21**, e3001983 (2023).
1165 73. Silva, J.G. *et al.* Emergence and fate of stem cell-like Tcf7(+) CD8(+) T cells during a
1166 primary immune response to viral infection. *Sci Immunol* **8**, eadh3113 (2023).
1167 74. Araki, K. *et al.* mTOR regulates memory CD8 T-cell differentiation. *Nature* **460**, 108-12
1168 (2009).
1169 75. Herndler-Brandstetter, D. *et al.* KLRG1(+) Effector CD8(+) T Cells Lose KLRG1,
1170 Differentiate into All Memory T Cell Lineages, and Convey Enhanced Protective
1171 Immunity. *Immunity* **48**, 716-729 e8 (2018).
1172 76. Crowl, J.T. *et al.* Tissue-resident memory CD8(+) T cells possess unique transcriptional,
1173 epigenetic and functional adaptations to different tissue environments. *Nat Immunol* **23**,
1174 1121-1131 (2022).
1175 77. Renkema, K.R. *et al.* KLRG1(+) Memory CD8 T Cells Combine Properties of Short-Lived
1176 Effectors and Long-Lived Memory. *J Immunol* **205**, 1059-1069 (2020).
1177 78. Abboud, G. *et al.* Transcription Factor Bcl11b Controls Effector and Memory CD8 T cell
1178 Fate Decision and Function during Poxvirus Infection. *Front Immunol* **7**, 425 (2016).
1179 79. Helm, E.Y. *et al.* Bcl11b sustains multipotency and restricts effector programs of
1180 intestinal-resident memory CD8(+) T cells. *Sci Immunol* **8**, eabn0484 (2023).
1181 80. Connolly, K.A. *et al.* A reservoir of stem-like CD8(+) T cells in the tumor-draining lymph
1182 node preserves the ongoing antitumor immune response. *Sci Immunol* **6**, eabg7836
1183 (2021).
1184 81. Escobar, G. *et al.* Tumor immunogenicity dictates reliance on TCF1 in CD8(+) T cells for
1185 response to immunotherapy. *Cancer Cell* **41**, 1662-1679 e7 (2023).
1186 82. Mazet, J.M. *et al.* IFNgamma signaling in cytotoxic T cells restricts anti-tumor responses
1187 by inhibiting the maintenance and diversity of intra-tumoral stem-like T cells. *Nat*
1188 *Commun* **14**, 321 (2023).
1189 83. Tabilas, C., Smith, N.L. & Rudd, B.D. Shaping immunity for life: Layered development of
1190 CD8(+) T cells. *Immunol Rev* **315**, 108-125 (2023).
1191 84. Wang, J. *et al.* Fetal and adult progenitors give rise to unique populations of CD8+ T
1192 cells. *Blood* **128**, 3073-3082 (2016).
1193 85. Chopp, L.B. *et al.* An Integrated Epigenomic and Transcriptomic Map of Mouse and
1194 Human alphabeta T Cell Development. *Immunity* **53**, 1182-1201 e8 (2020).
1195 86. Steier, Z. *et al.* Single-cell multiomic analysis of thymocyte development reveals drivers
1196 of CD4(+) T cell and CD8(+) T cell lineage commitment. *Nat Immunol* **24**, 1579-1590
1197 (2023).
1198 87. Cyster, J.G. & Schwab, S.R. Sphingosine-1-phosphate and lymphocyte egress from
1199 lymphoid organs. *Annu Rev Immunol* **30**, 69-94 (2012).
1200 88. Hosokawa, H. *et al.* Bcl11b sets pro-T cell fate by site-specific cofactor recruitment and
1201 by repressing Id2 and Zbtb16. *Nat Immunol* **19**, 1427-1440 (2018).

1202 89. Mack, R., Zhang, L., Breslin Sj, P. & Zhang, J. The Fetal-to-Adult Hematopoietic Stem
1203 Cell Transition and its Role in Childhood Hematopoietic Malignancies. *Stem Cell Rev*
1204 *Rep* **17**, 2059-2080 (2021).
1205 90. Heo, I. *et al.* Lin28 mediates the terminal uridylation of let-7 precursor MicroRNA. *Mol*
1206 *Cell* **32**, 276-84 (2008).
1207 91. Yuan, J., Nguyen, C.K., Liu, X., Kanellopoulou, C. & Muljo, S.A. Lin28b reprograms adult
1208 bone marrow hematopoietic progenitors to mediate fetal-like lymphopoiesis. *Science*
1209 **335**, 1195-200 (2012).
1210 92. Wells, A.C. *et al.* Modulation of let-7 miRNAs controls the differentiation of effector CD8
1211 T cells. *Elife* **6**(2017).
1212 93. Horr, B. *et al.* Production and characterization of monoclonal antibodies to Xenopus
1213 proteins. *Development* **150**(2023).
1214 94. Hao, Y. *et al.* Integrated analysis of multimodal single-cell data. *Cell* **184**, 3573-3587 e29
1215 (2021).
1216 95. Contreras, A. *et al.* Co-transfer of tumor-specific effector and memory CD8+ T cells
1217 enhances the efficacy of adoptive melanoma immunotherapy in a mouse model. *J*
1218 *Immunother Cancer* **6**, 41 (2018).
1219 96. Love, M.I., Huber, W. & Anders, S. Moderated estimation of fold change and dispersion
1220 for RNA-seq data with DESeq2. *Genome Biol* **15**, 550 (2014).
1221 97. Zhou, Y. *et al.* Metascape provides a biologist-oriented resource for the analysis of
1222 systems-level datasets. *Nat Commun* **10**, 1523 (2019).
1223

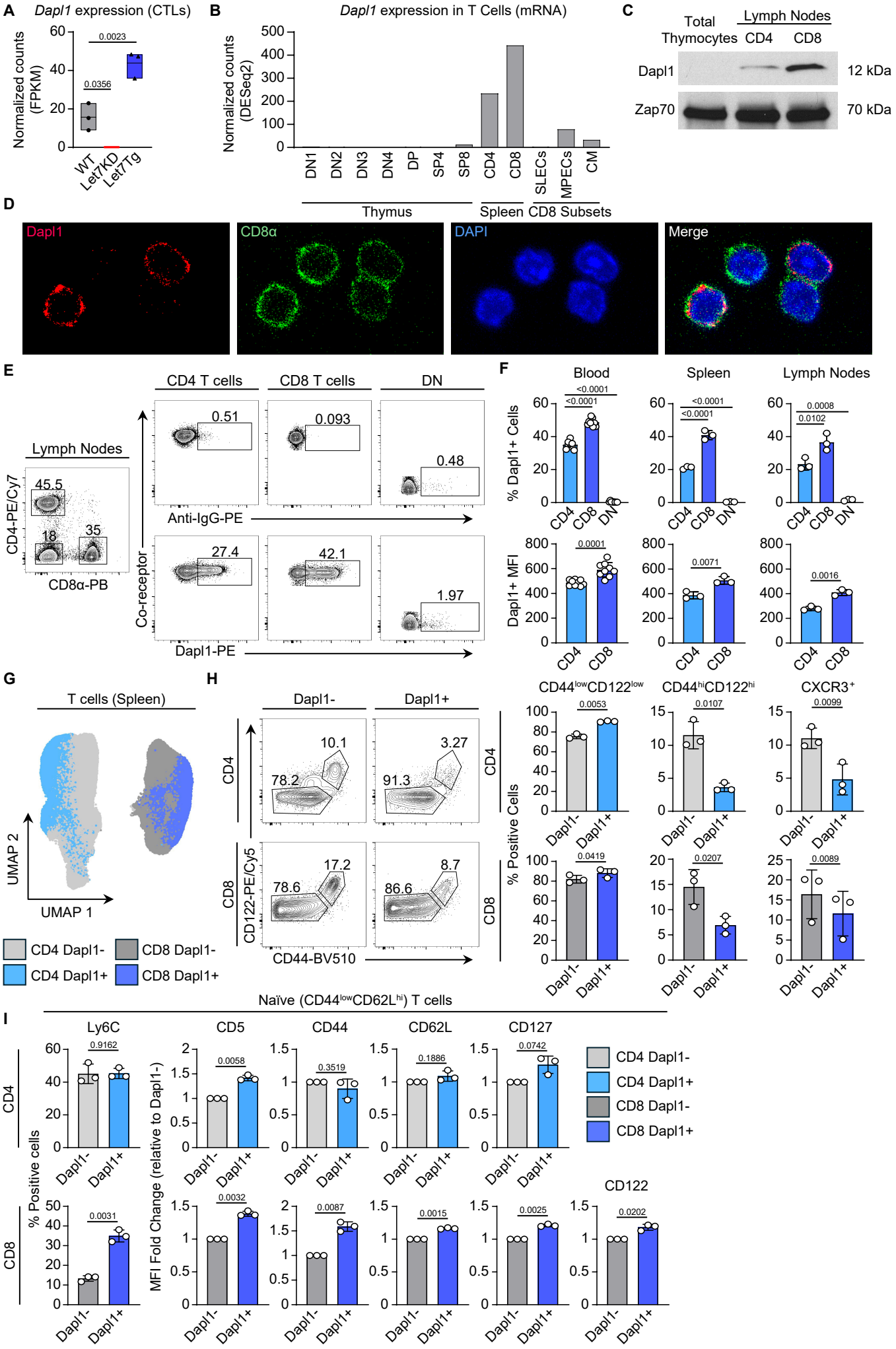
A
Dapl1 expression (CTLs)
Normalized counts (FPKM)
0.0023
0.0356
WT
Let7KD
Let7Tg
B
Dapl1 expression in T Cells (mRNA)
Normalized counts (DESeq2)
DN1
DN2
DN3
DN4
DP
SP4
SP8
CD4
CD8
SLECs
MPECs
CM
Thymus
Spleen
CD8 Subsets
C
Total Thymocytes
Lymph Nodes
CD4
CD8
Dapl1
Zap70
12 kDa
70 kDa
D
Dapl1
CD8α
DAPI
Merge
E
CD4 T cells
CD8 T cells
DN
Lymph Nodes
45.5
18
35
CD4-PE/Cy7
CD8α-PB
0.51
0.093
0.48
Anti-IgG-PE
27.4
42.1
1.97
Co-receptor
Dapl1-PE
F
Blood
Spleen
Lymph Nodes
% Dapl1+ Cells
<0.0001
<0.0001
<0.0001
<0.0001
0.0008
0.0102
Dapl1+ MFI
0.0001
0.0071
0.0016
G
T cells (Spleen)
UMAP 2
UMAP 1
CD4 Dapl1-
CD4 Dapl1+
CD8 Dapl1-
CD8 Dapl1+
H
Dapl1-
Dapl1+
CD4
CD8
10.1
78.2
3.27
91.3
17.2
78.6
8.7
86.6
CD122-PE/Cy5
CD44-BV510
CD44lowCD122low
CD44hiCD122hi
CXCR3+
% Positive Cells
0.0053
0.0107
0.0099
0.0419
0.0207
0.0089
Naïve (CD44lowCD62Lhi) T cells
I
Ly6C
CD5
CD44
CD62L
CD127
CD122
% Positive cells
MFI Fold Change (relative to Dapl1-)
0.9162
0.0058
0.3519
0.1886
0.0742
0.0031
0.0032
0.0087
0.0015
0.0025
0.0202
CD4 Dapl1-
CD4 Dapl1+
CD8 Dapl1-
CD8 Dapl1+

Figure 1

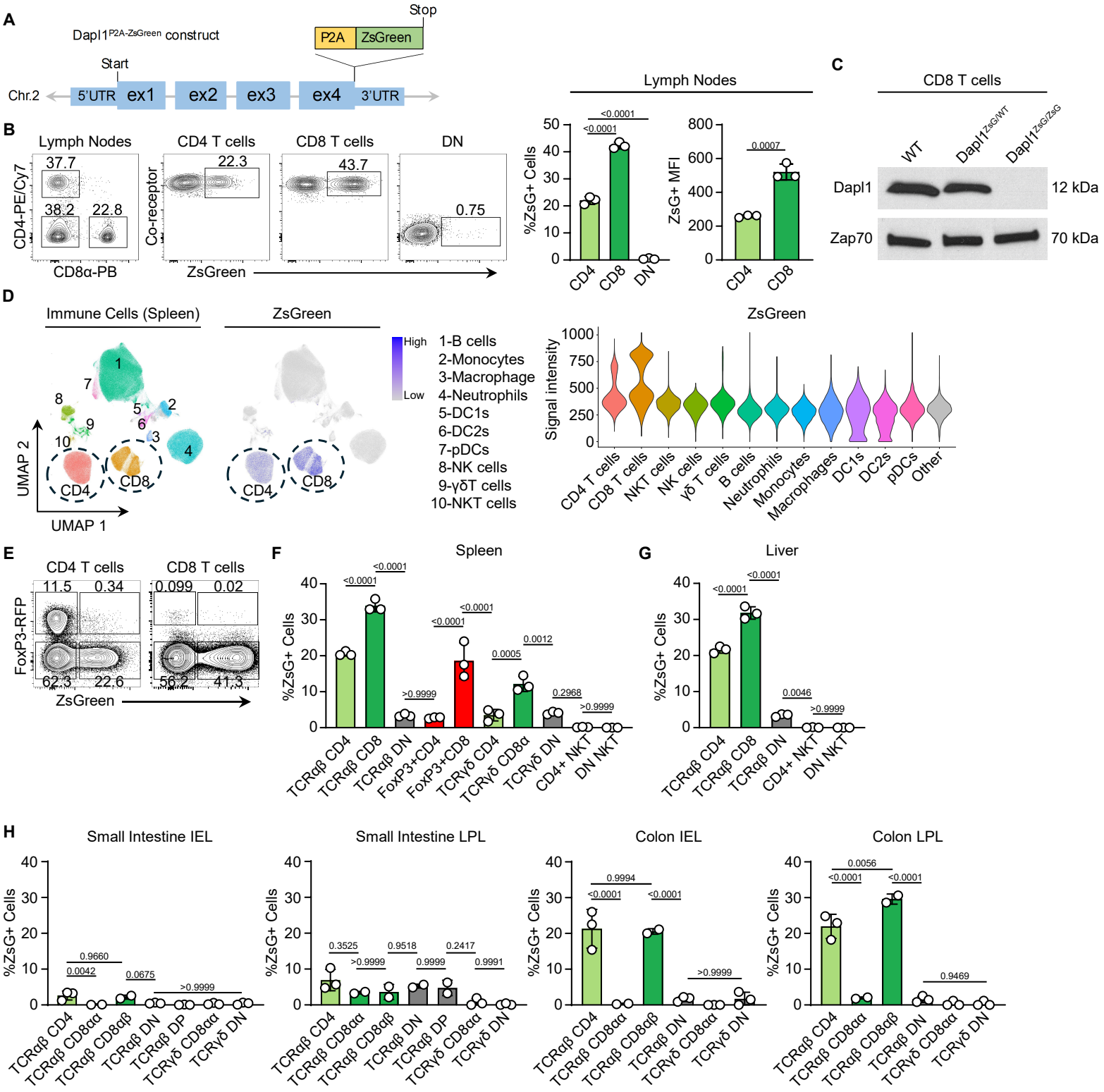
A
Dapl1P2A-ZsGreen construct
Stop
P2A
ZsGreen
Start
Chr.2
5'UTR
ex1
ex2
ex3
ex4
3'UTR
B
Lymph Nodes
CD4 T cells
CD8 T cells
DN
37.7
38.2
22.8
22.3
43.7
0.75
CD4-PE/Cy7
CD8α-PB
Co-receptor
ZsGreen
Lymph Nodes
%ZsG+ Cells
<0.0001
<0.0001
ZsG+ MFI
0.0007
CD4
CD8
DN
C
CD8 T cells
WT
Dapl1ZsG/WT
Dapl1ZsG/ZsG
Dapl1
12 kDa
Zap70
70 kDa
D
Immune Cells (Spleen)
ZsGreen
High
Low
UMAP 2
UMAP 1
CD4
CD8
1-B cells
2-Monocytes
3-Macrophage
4-Neutrophils
5-DC1s
6-DC2s
7-pDCs
8-NK cells
9-γδT cells
10-NKT cells
ZsGreen
Signal intensity
CD4 T cells
CD8 T cells
NKT cells
NK cells
γδ T cells
B cells
Neutrophils
Monocytes
Macrophages
DC1s
DC2s
pDCs
Other
E
CD4 T cells
CD8 T cells
11.5
0.34
62.3
22.6
0.099
0.02
56.2
41.3
FoxP3-RFP
ZsGreen
F
Spleen
%ZsG+ Cells
<0.0001
<0.0001
>0.9999
<0.0001
<0.0001
0.0005
0.0012
0.2968
>0.9999
TCRαβ CD4
TCRαβ CD8
TCRαβ DN
FoxP3+CD4
FoxP3+CD8
TCRγδ CD4
TCRγδ CD8α
TCRγδ DN
CD4+ NKT
DN NKT
G
Liver
%ZsG+ Cells
<0.0001
<0.0001
0.0046
>0.9999
TCRαβ CD4
TCRαβ CD8
TCRαβ DN
CD4+ NKT
DN NKT
H
Small Intestine IEL
Small Intestine LPL
Colon IEL
Colon LPL
%ZsG+ Cells
0.9660
0.0042
0.0675
>0.9999
0.3525
>0.9999
0.9518
0.9999
0.2417
0.9991
0.9994
<0.0001
<0.0001
>0.9999
0.0056
<0.0001
<0.0001
0.9469
TCRαβ CD4
TCRαβ CD8αα
TCRαβ CD8αβ
TCRαβ DN
TCRαβ DP
TCRγδ CD8αα
TCRγδ DN

Figure 2

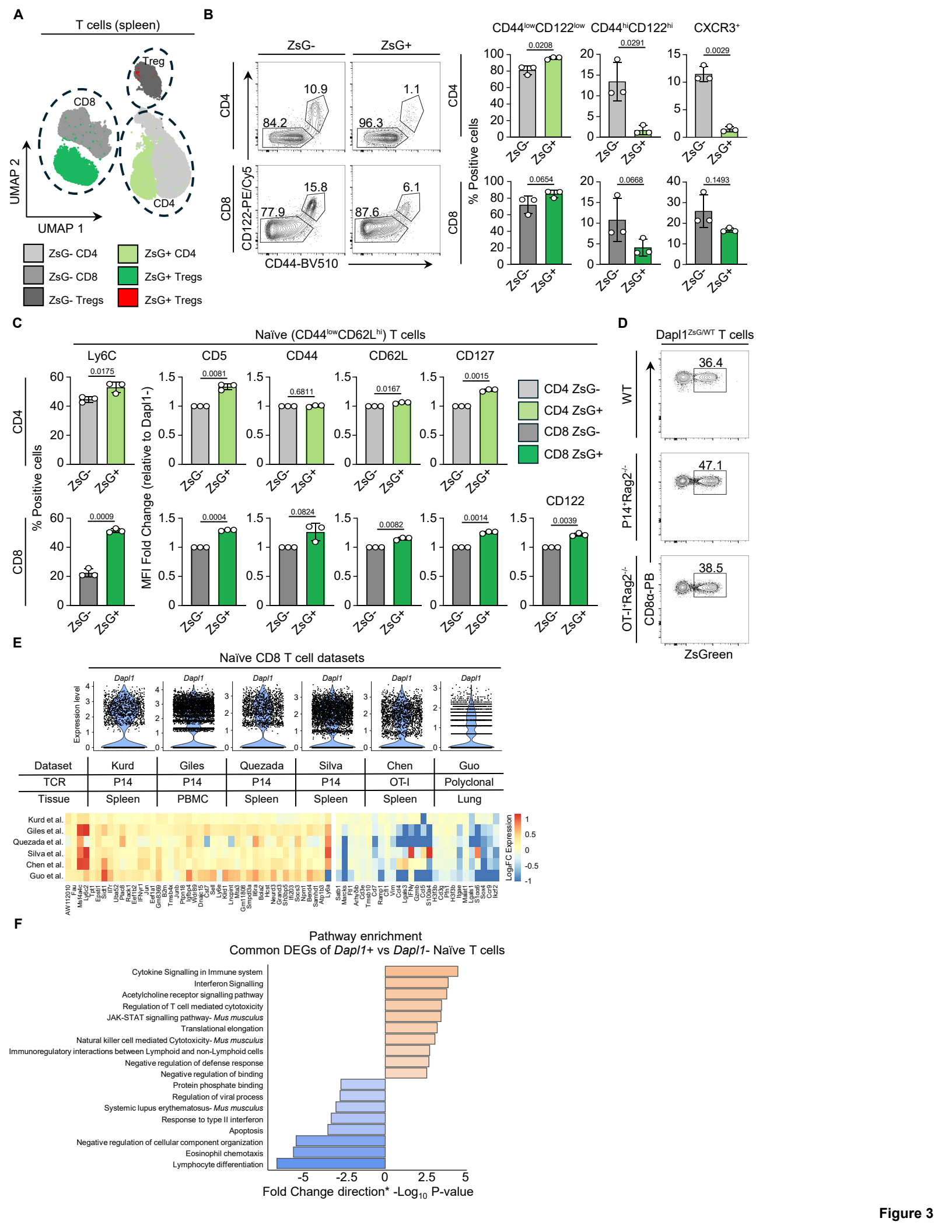
A
T cells (spleen)
Treg
CD8
CD4
UMAP 2
UMAP 1
ZsG- CD4
ZsG- CD8
ZsG- Tregs
ZsG+ CD4
ZsG+ Tregs
ZsG+ Tregs
B
ZsG-
ZsG+
CD4
CD8
10.9
84.2
1.1
96.3
15.8
77.9
6.1
87.6
CD122-PE/Cy5
CD44-BV510
CD44lowCD122low
CD44hiCD122hi
CXCR3+
% Positive cells
0.0208
0.0291
0.0029
0.0654
0.0668
0.1493
C
Naïve (CD44lowCD62Lhi) T cells
Ly6C
CD5
CD44
CD62L
CD127
CD122
% Positive cells
MFI Fold Change (relative to Dapl1-)
0.0175
0.0081
0.6811
0.0167
0.0015
0.0009
0.0004
0.0824
0.0082
0.0014
0.0039
CD4 ZsG-
CD4 ZsG+
CD8 ZsG-
CD8 ZsG+
D
Dapl1ZsG/WT T cells
WT
P14+Rag2-/-
OT-I+Rag2-/-
CD8α-PB
36.4
47.1
38.5
ZsGreen
E
Naïve CD8 T cell datasets
Dapl1
Expression level
Dataset
Kurd
Giles
Quezada
Silva
Chen
Guo
TCR
P14
P14
P14
P14
OT-I
Polyclonal
Tissue
Spleen
PBMC
Spleen
Spleen
Spleen
Lung
Kurd et al.
Giles et al.
Quezada et al.
Silva et al.
Chen et al.
Guo et al.
LogFC Expression
F
Pathway enrichment
Common DEGs of Dapl1+ vs Dapl1- Naïve T cells
Cytokine Signalling in Immune system
Interferon Signalling
Acetylcholine receptor signalling pathway
Regulation of T cell mediated cytotoxicity
JAK-STAT signalling pathway- Mus musculus
Translational elongation
Natural killer cell mediated Cytotoxicity- Mus musculus
Immunoregulatory interactions between Lymphoid and non-Lymphoid cells
Negative regulation of defense response
Negative regulation of binding
Protein phosphate binding
Regulation of viral process
Systemic lupus erythematosus- Mus musculus
Response to type II interferon
Apoptosis
Negative regulation of cellular component organization
Eosinophil chemotaxis
Lymphocyte differentiation
Fold Change direction* -Log10 P-value

Figure 3

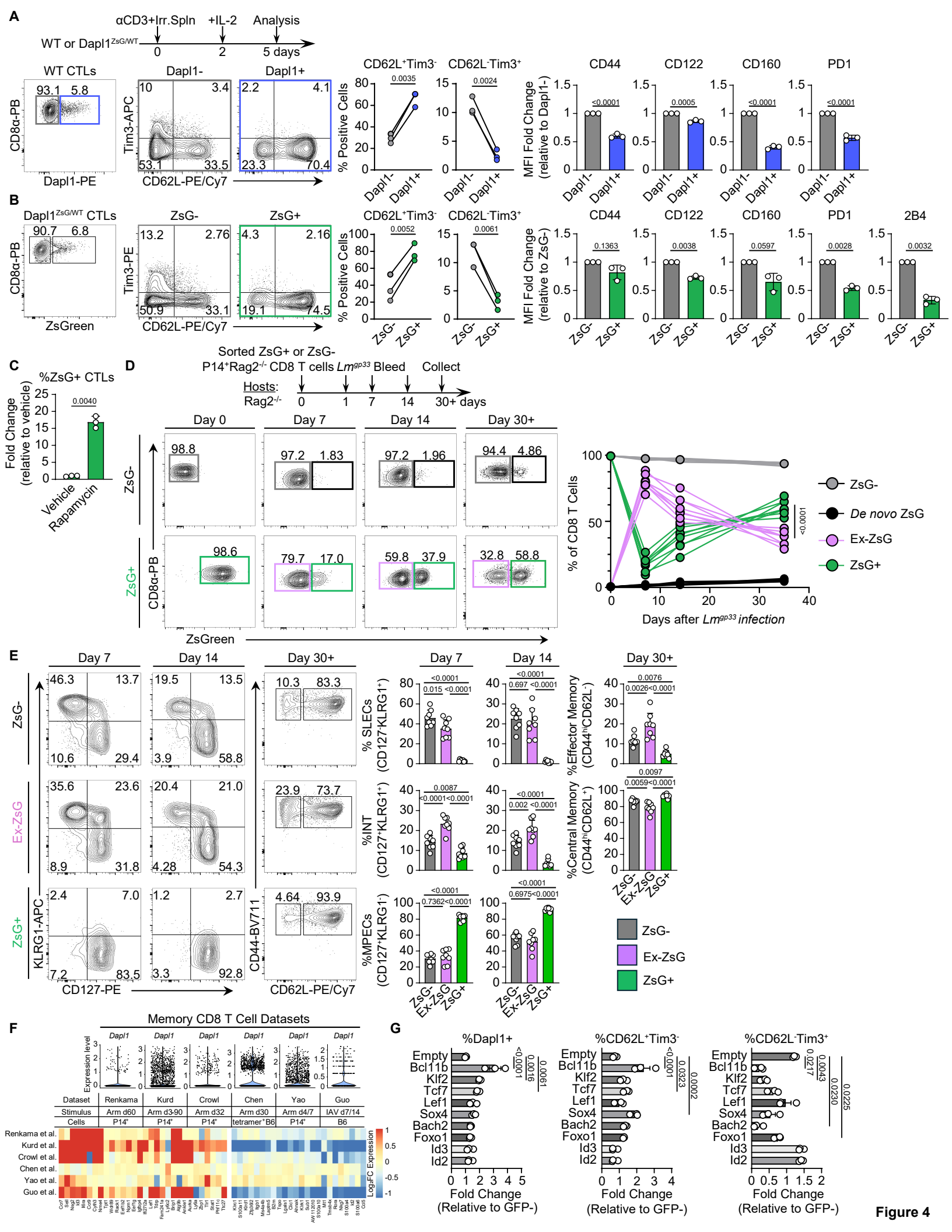
A
αCD3+Irr.Spln
+IL-2
Analysis
WT or Dapl1ZsG/WT
0
2
5 days
WT CTLs
Dapl1-
Dapl1+
CD8α-PB
Dapl1-PE
Tim3-APC
CD62L-PE/Cy7
% Positive Cells
MFI Fold Change (relative to Dapl1-)
CD44
CD122
CD160
PD1
B
Dapl1ZsG/WT CTLs
ZsG-
ZsG+
CD8α-PB
ZsGreen
Tim3-PE
CD62L-PE/Cy7
MFI Fold Change (relative to ZsG-)
2B4
C
%ZsG+ CTLs
Fold Change (relative to vehicle)
Vehicle
Rapamycin
D
Sorted ZsG+ or ZsG- P14+Rag2-/- CD8 T cells
Lmgp33 Bleed
Collect
Hosts: Rag2-/-
0
1
7
14
30+ days
Day 0
Day 7
Day 14
Day 30+
ZsGreen
% of CD8 T Cells
Days after Lmgp33 infection
ZsG-
De novo ZsG
Ex-ZsG
ZsG+
E
KLRG1-APC
CD127-PE
CD44-BV711
CD62L-PE/Cy7
% SLECs (CD127+KLRG1+)
%INT (CD127+KLRG1-)
%MPECs (CD127-KLRG1-)
%Effector Memory (CD44hiCD62L-)
%Central Memory (CD44hiCD62L+)
F
Memory CD8 T Cell Datasets
Expression level
Dataset
Renkama
Kurd
Crowl
Chen
Yao
Guo
Stimulus
Arm d60
Arm d3-90
Arm d32
Arm d30
Arm d4/7
IAV d7/14
Cells
P14+
tetramer+B6
B6
Renkama et al.
Kurd et al.
Crowl et al.
Chen et al.
Yao et al.
Guo et al.
Log2FC Expression
G
%Dapl1+
%CD62L+Tim3-
%CD62L-Tim3+
Empty
Bcl11b
Klf2
Tcf7
Lef1
Sox4
Bach2
Foxo1
Id3
Id2
Fold Change (Relative to GFP-)

Figure 4

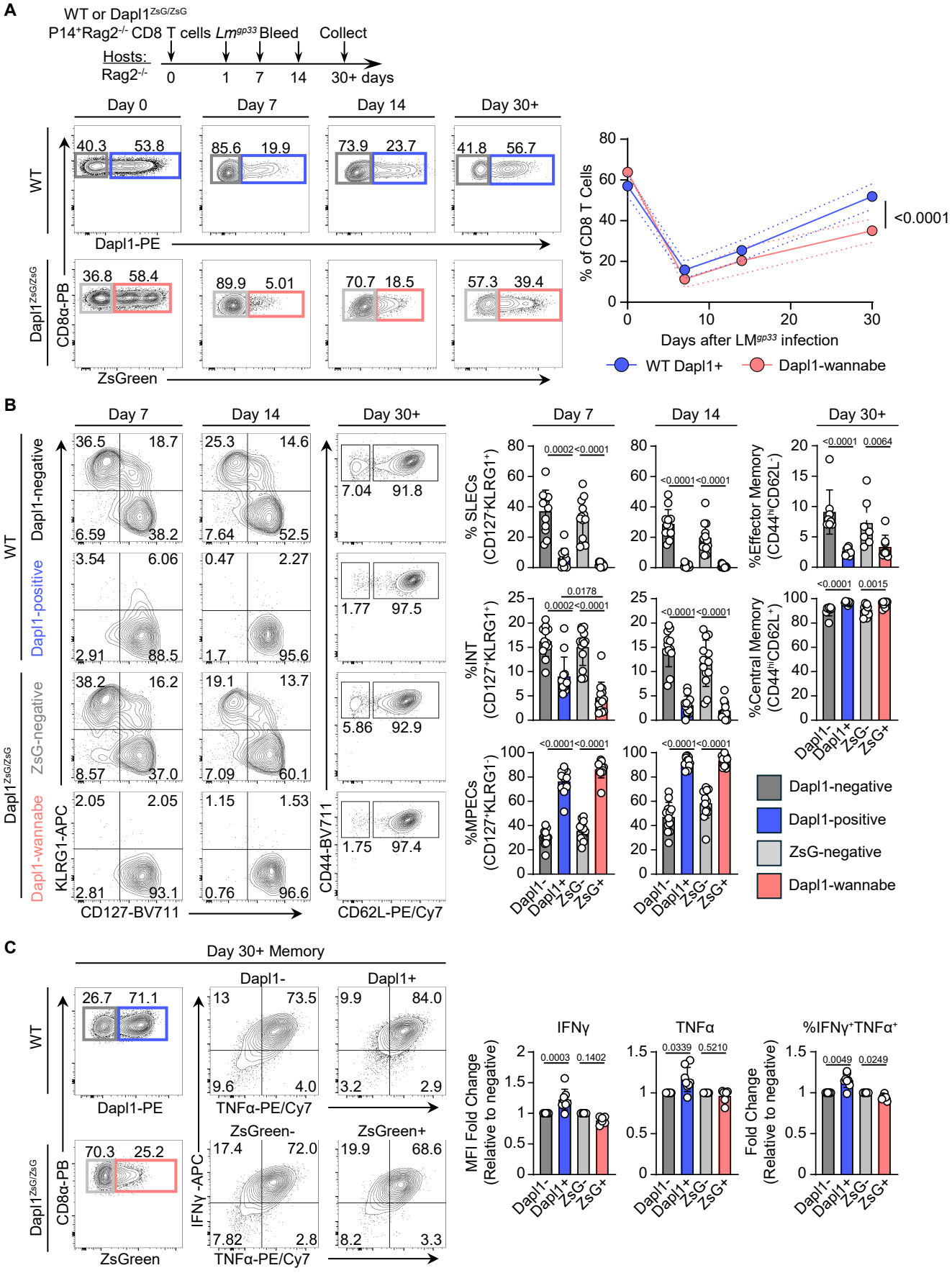
A
WT or Dapl1ZsG/ZsG
P14+Rag2-/- CD8 T cells Lmgp33 Bleed Collect
Hosts: Rag2-/-
0 1 7 14 30+ days
Day 0
Day 7
Day 14
Day 30+
WT
Dapl1ZsG/ZsG
Dapl1-PE
CD8α-PB
ZsGreen
% of CD8 T Cells
Days after LMgp33 infection
<0.0001
WT Dapl1+
Dapl1-wannabe
B
Dapl1-negative
Dapl1-positive
ZsG-negative
Dapl1-wannabe
KLRG1-APC
CD127-BV711
CD44-BV711
CD62L-PE/Cy7
% SLECs (CD127+KLRG1+)
%INT (CD127+KLRG1+)
%MPECs (CD127+KLRG1-)
%Effector Memory (CD44hiCD62L-)
%Central Memory (CD44hiCD62L+)
Dapl1-
Dapl1+
ZsG-
ZsG+
C
Day 30+ Memory
Dapl1-
Dapl1+
ZsGreen-
ZsGreen+
TNFα-PE/Cy7
IFNγ-APC
IFNγ
TNFα
%IFNγ+TNFα+
MFI Fold Change (Relative to negative)
Fold Change (Relative to negative)

Figure 5

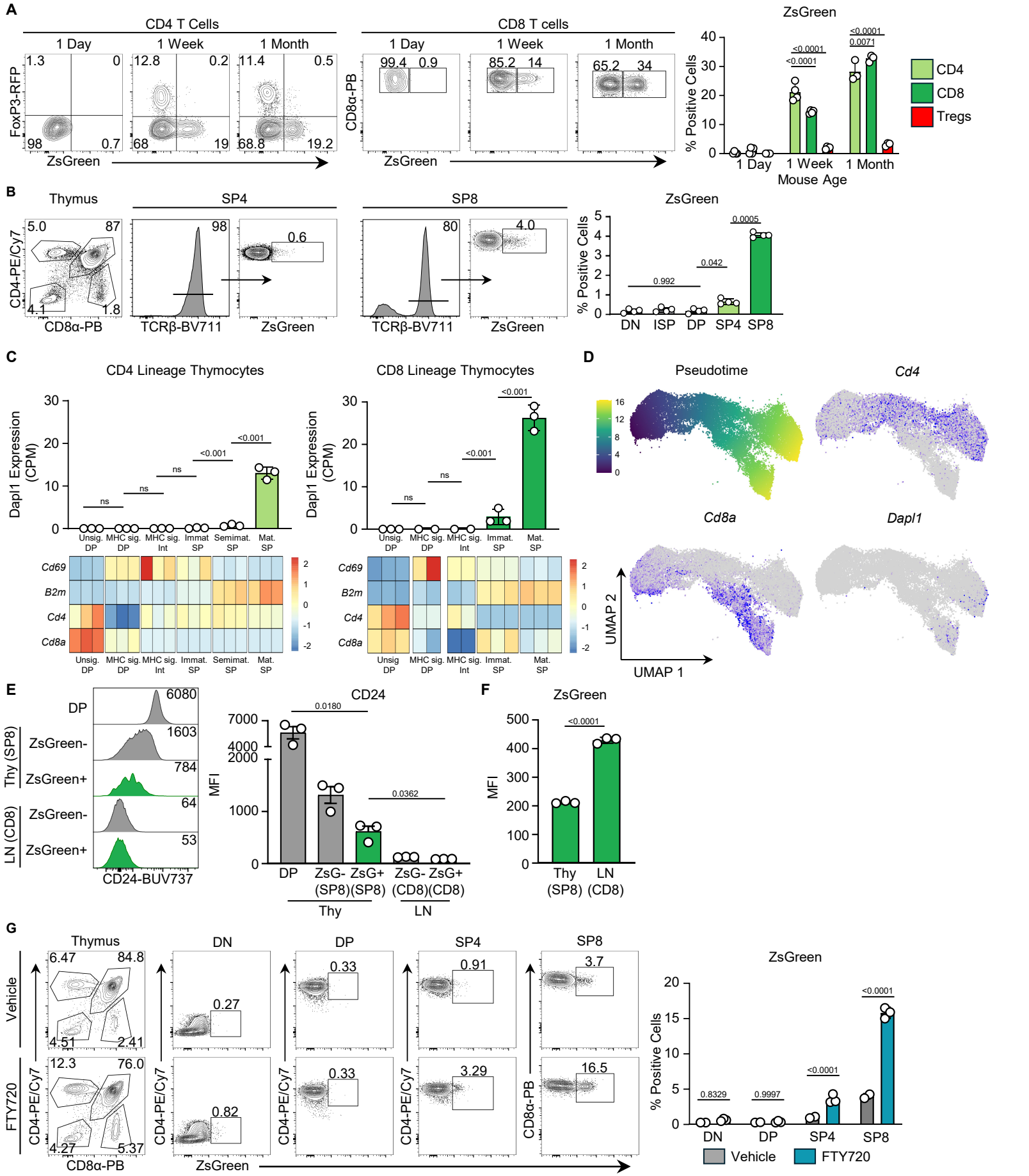
A
CD4 T Cells
1 Day
1 Week
1 Month
FoxP3-RFP
ZsGreen
1.3
0
98
0.7
12.8
0.2
68
19
11.4
0.5
68.8
19.2
CD8 T cells
CD8α-PB
99.4
0.9
85.2
14
65.2
34
ZsGreen
% Positive Cells
Mouse Age
<0.0001
<0.0001
<0.0001
0.0071
CD4
CD8
Tregs
B
Thymus
SP4
SP8
CD4-PE/Cy7
CD8α-PB
TCRβ-BV711
ZsGreen
5.0
87
4.1
1.8
98
0.6
80
4.0
% Positive Cells
0.992
0.042
0.0005
DN
ISP
DP
SP4
SP8
C
CD4 Lineage Thymocytes
CD8 Lineage Thymocytes
Dapl1 Expression (CPM)
ns
ns
ns
<0.001
<0.001
<0.001
<0.001
Unsig. DP
MHC sig. DP
MHC sig. Int
Immat. SP
Semimat. SP
Mat. SP
Cd69
B2m
Cd4
Cd8a
D
Pseudotime
Cd4
Cd8a
Dapl1
UMAP 2
UMAP 1
E
DP
ZsGreen-
ZsGreen+
Thy (SP8)
LN (CD8)
6080
1603
784
64
53
CD24-BUV737
CD24
MFI
0.0180
0.0362
DP
ZsG- (SP8)
ZsG+ (SP8)
ZsG- (CD8)
ZsG+ (CD8)
Thy
LN
F
ZsGreen
<0.0001
Thy (SP8)
LN (CD8)
G
Thymus
DN
DP
SP4
SP8
Vehicle
FTY720
6.47
84.8
4.51
2.41
12.3
76.0
4.27
5.37
0.27
0.82
0.33
0.33
0.91
3.29
3.7
16.5
CD8α-PB
ZsGreen
% Positive Cells
0.8329
0.9997
<0.0001
<0.0001
Vehicle
FTY720

Figure 6

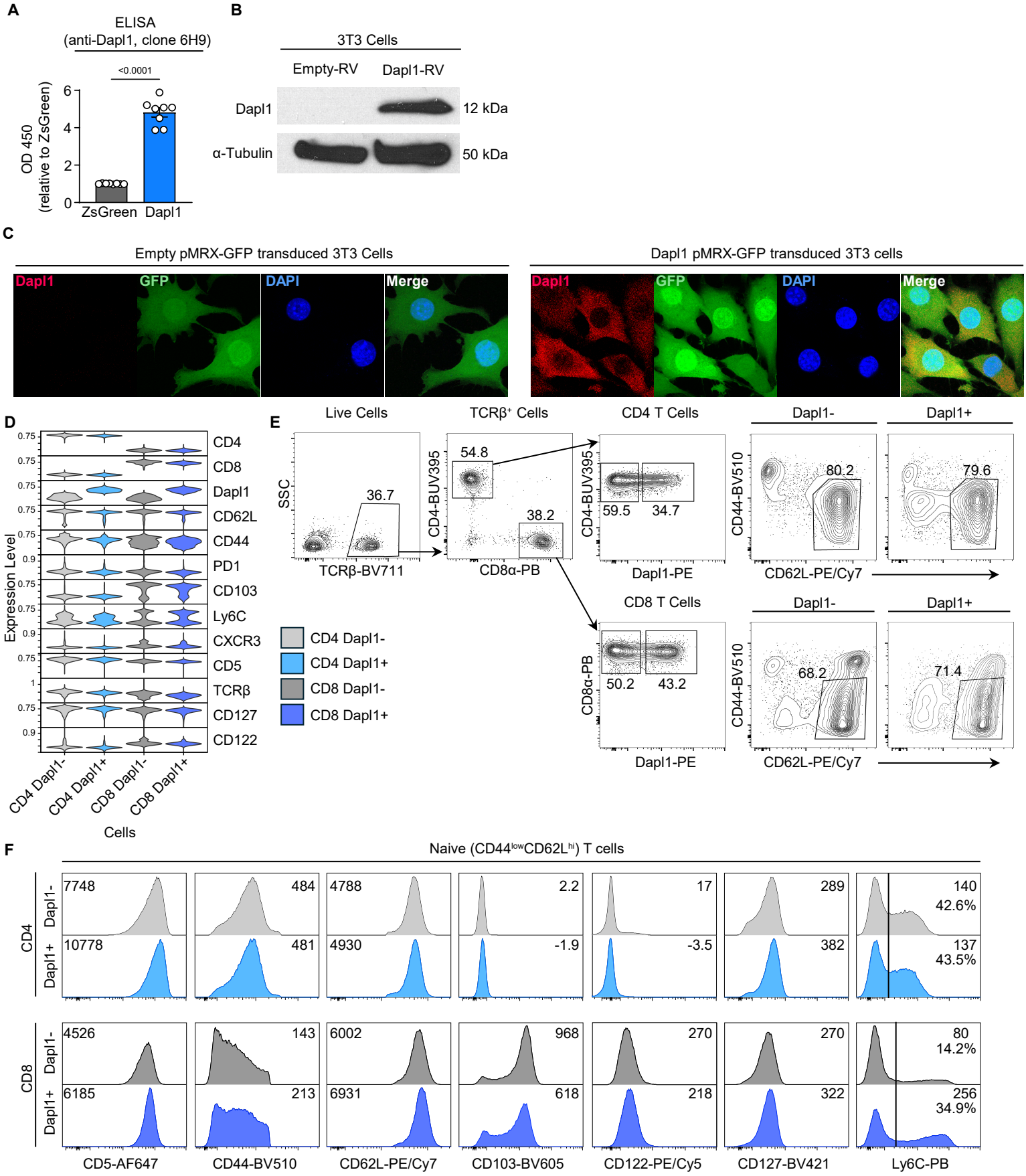

Supplementary Figure 1

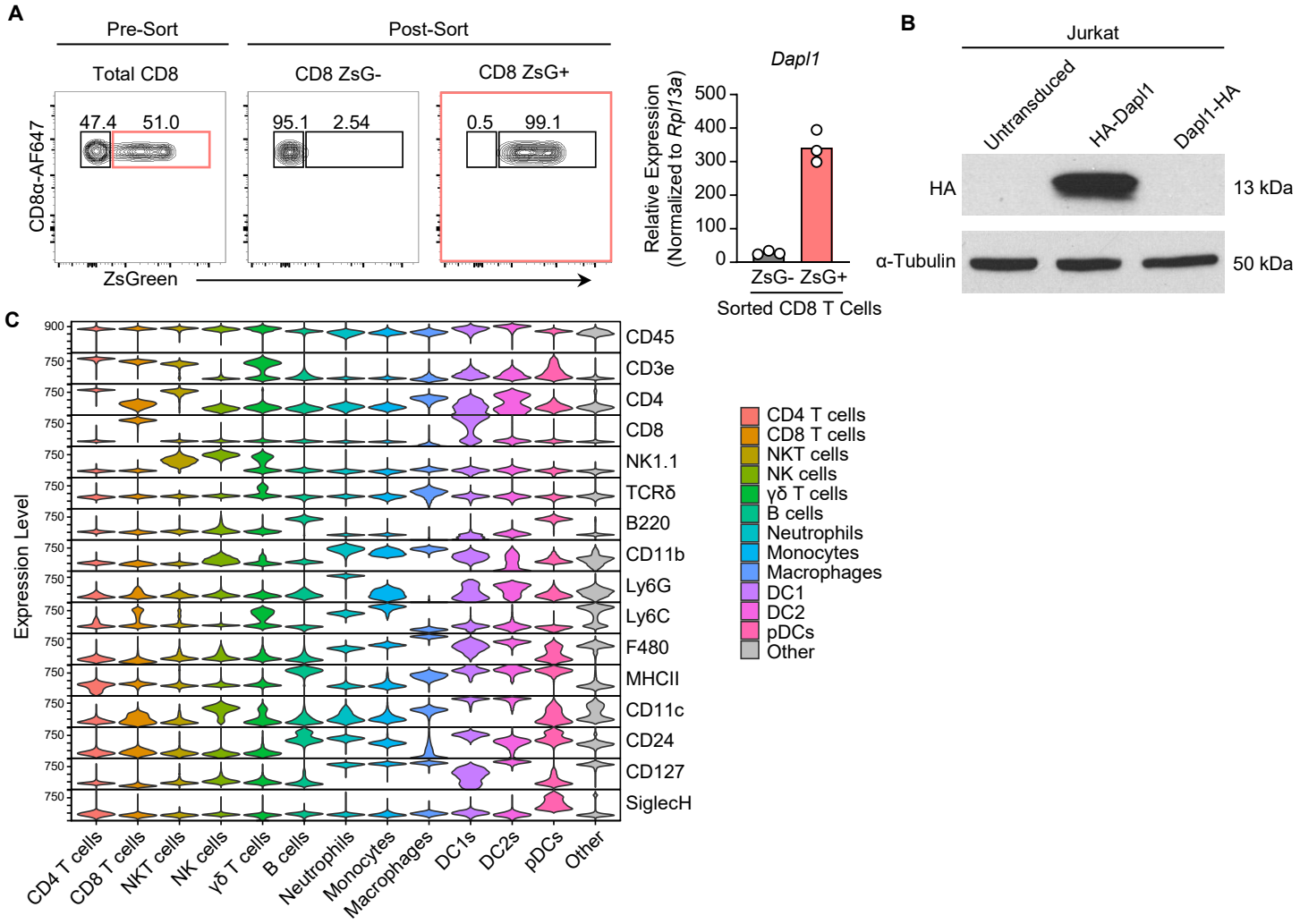

Supplementary Figure 2

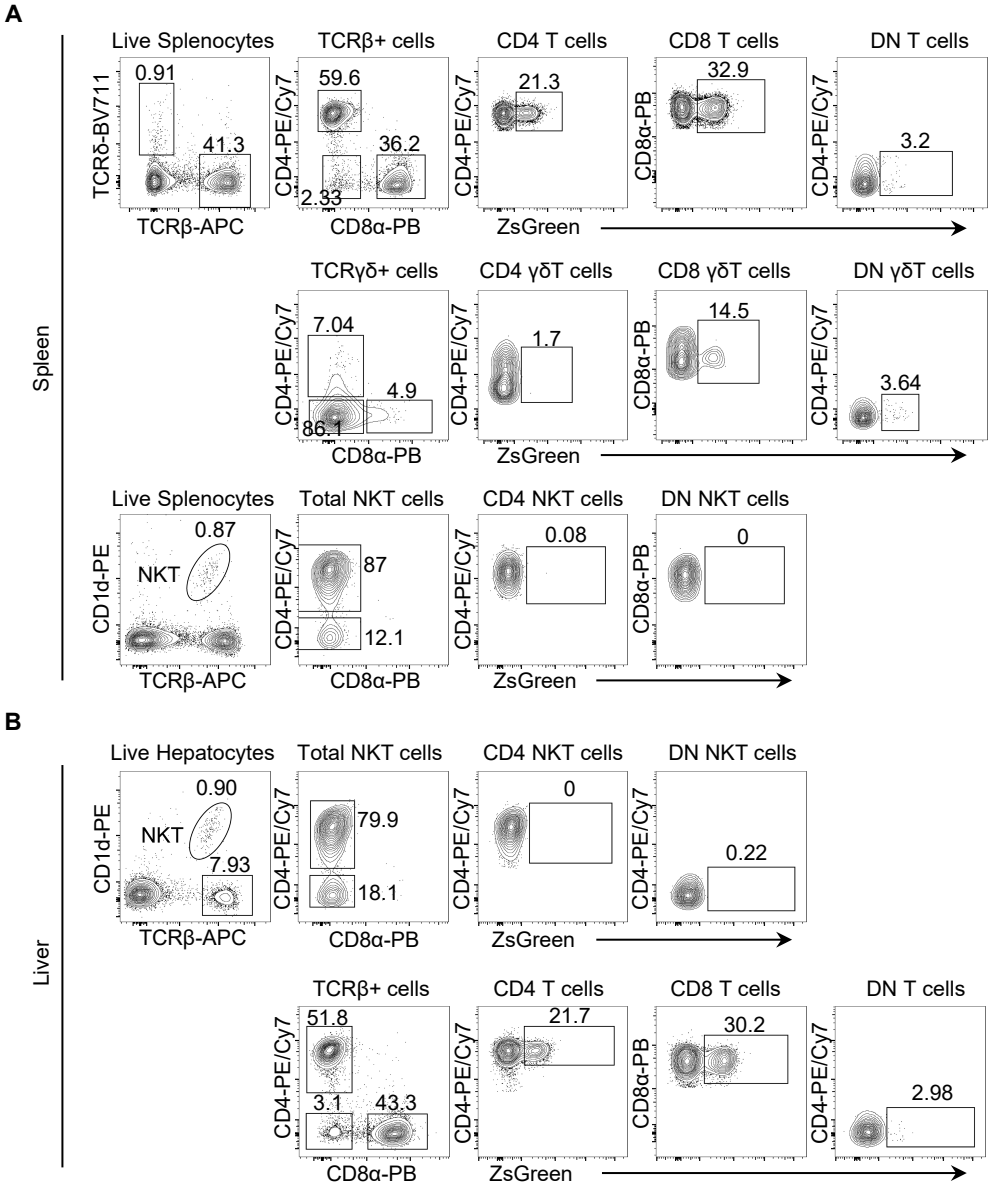

Supplementary Figure 3

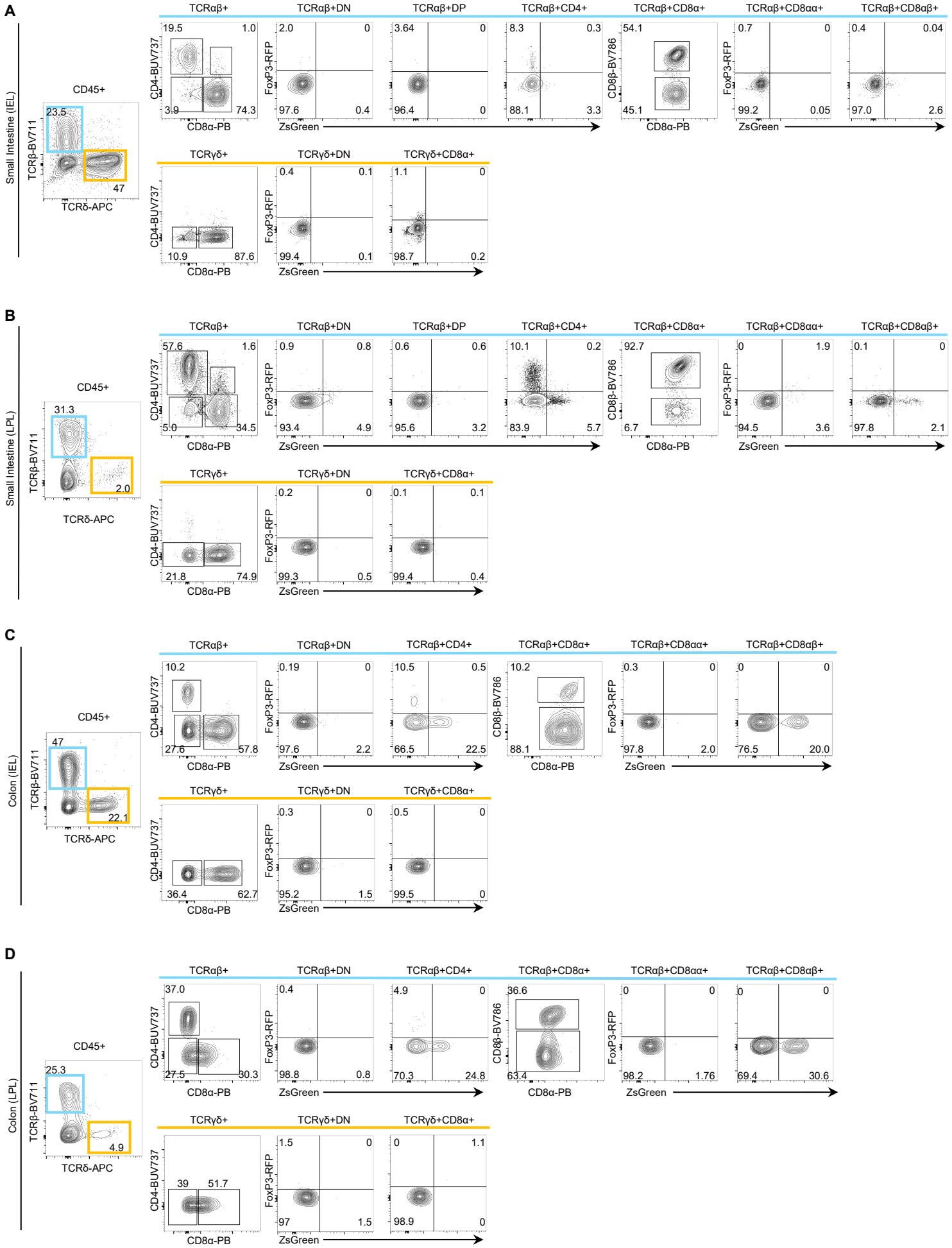

Supplementary Figure 4

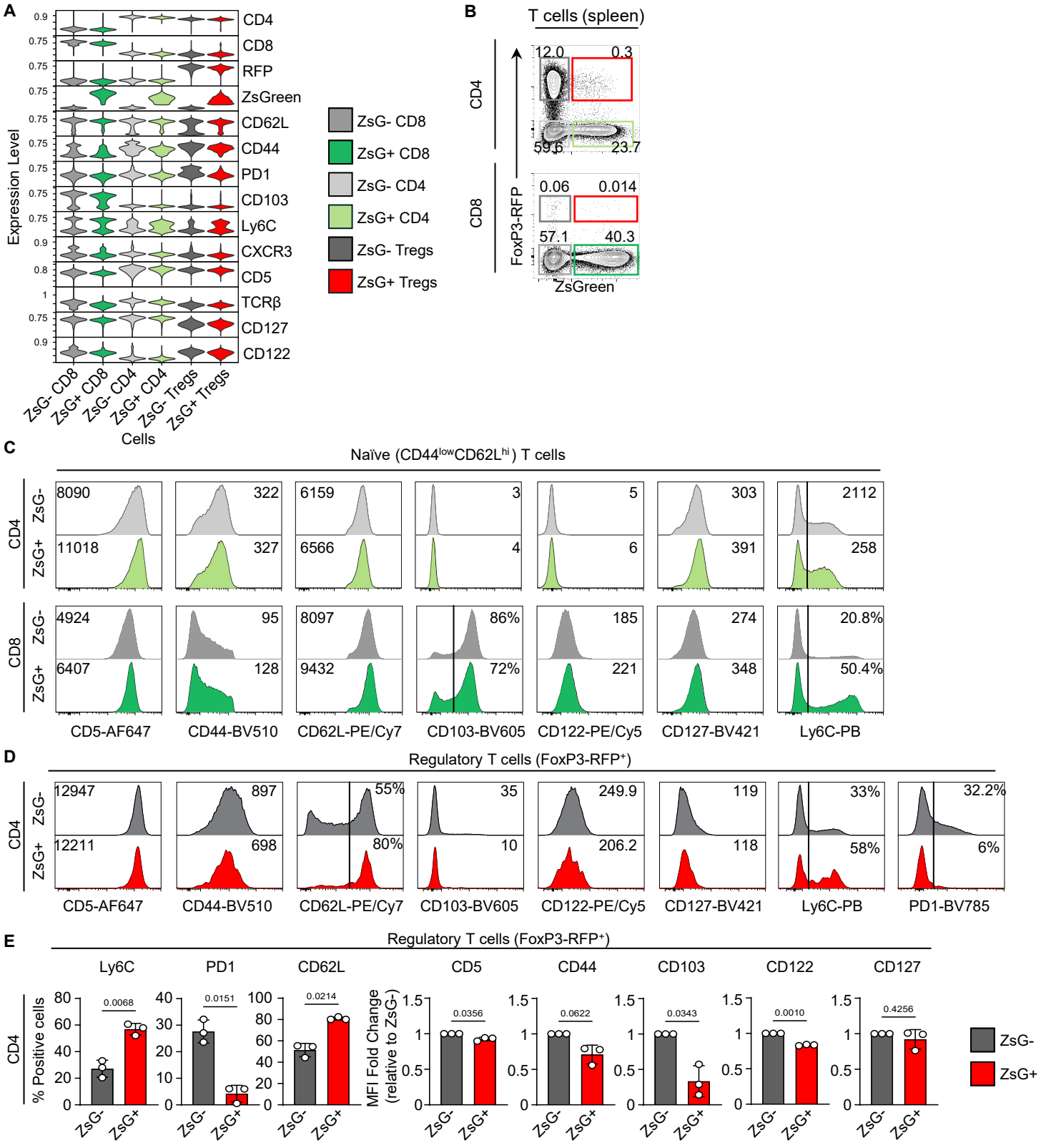

Supplementary Figure 5

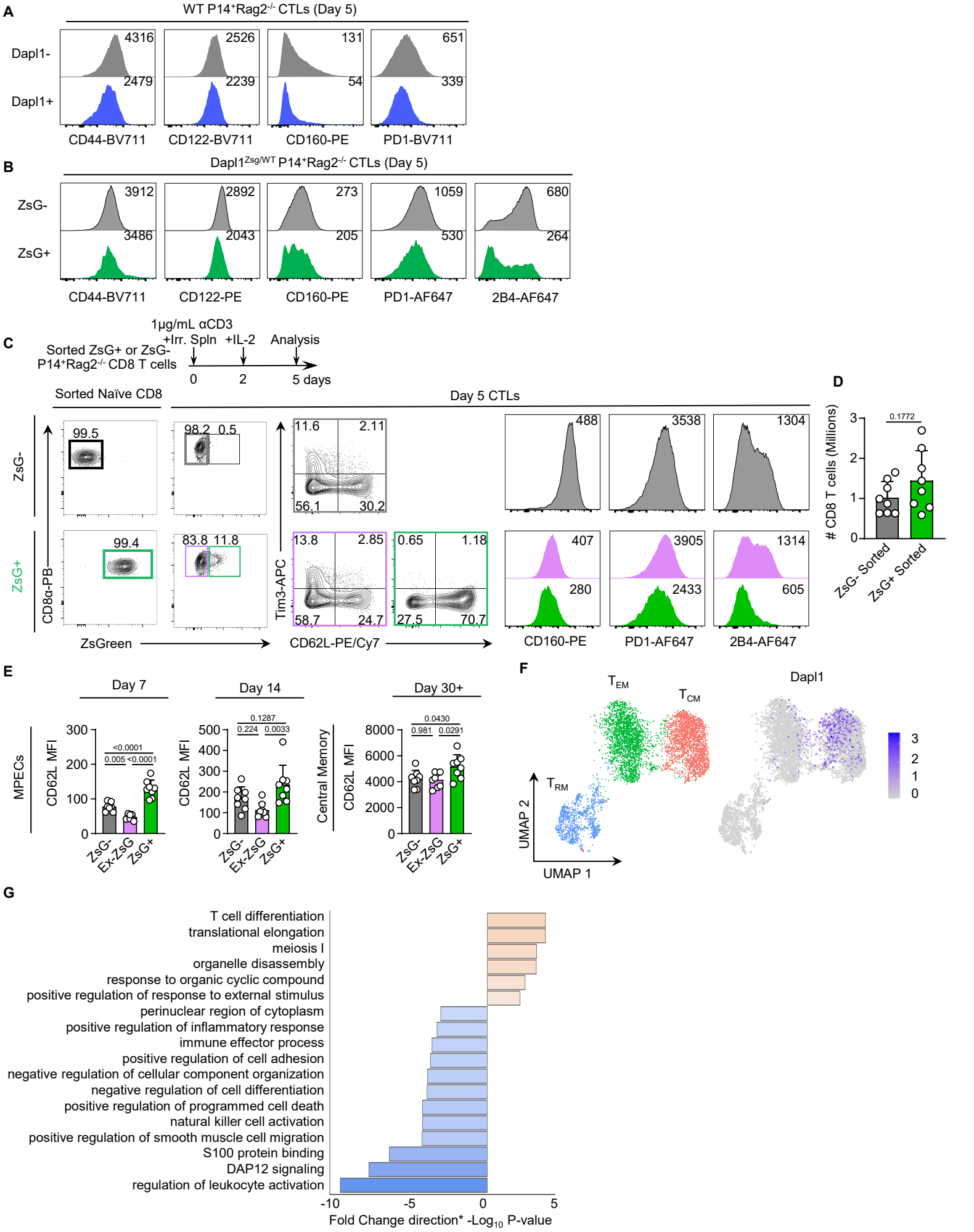

Supplementary figure 6

A

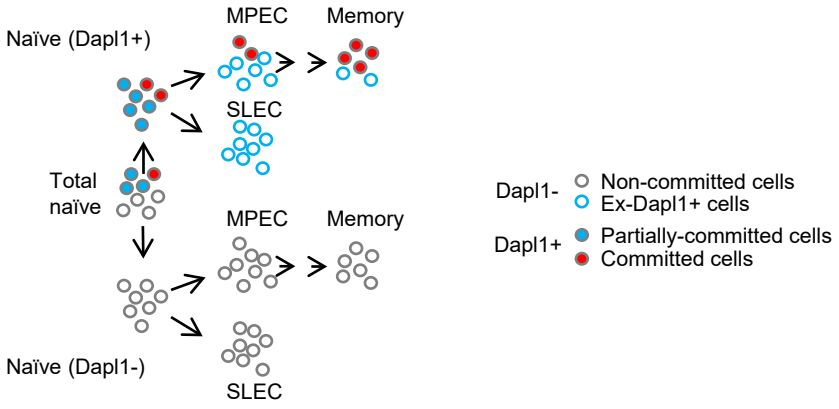

Supplementary figure 7

A

P14+Rag2-/-CTLs

Empty-RV: 70.8 28.1; GFP- 24; GFP+ 21; GFP- 12.7 4.39 46.4 36.5; GFP+ 16.2 6.33 50.2 27.3

Bcl11b-RV: 98.0 1.49; GFP- 29.7; GFP+ 70.1; GFP- 5.63 2.91 41.8 49.7; GFP+ 0.45 2.31 4.58 92.7

Klf2-RV: 85.2 14.3; GFP- 18.2; GFP+ 37.9; GFP- 18.3 5.61 45.1 31; GFP+ 6.98 47.5 6.87 38.7

Tcf7-RV: 97.2 2.22; GFP- 17.4; GFP+ 32.9; GFP- 10.6 2.9 56.3 30.2; GFP+ 6.33 6.05 42.2 45.5

Lef1-RV: 93.1 5.83; GFP- 20.8; GFP+ 36.9; GFP- 14.8 3.94 51.6 29.7; GFP+ 11.8 6.69 48.7 32.9

Sox4-RV: 98.2 1.47; GFP- 12.1; GFP+ 16.4; GFP- 31.1 4.27 43.1 21.5; GFP+ 13.9 6.3 35.3 44.5

Foxo1-RV: 96.5 2.81; GFP- 18.4; GFP+ 24.8; GFP- 11.6 3.46 51.1 33.9; GFP+ 8.95 10.3 36.6 44.2

Id3-RV: 56.4 42.8; GFP- 11.1; GFP+ 13.7; GFP- 26.5 3.74 48.6 21.1; GFP+ 36.8 4.8 45.2 13.3

Id2-RV: 57.9 41.0; GFP- 10.2; GFP+ 12.4; GFP- 27.7 4.18 47.5 20.7; GFP+ 37.6 5.54 44.3 12.6

Bach2-RV: 92.4 6.78; GFP- 29.8; GFP+ 42; GFP- 6.82 3.38 44.7 45.1; GFP+ 0.96 1.94 32.9 64.2

CD8α-PB; GFP; Dapl1-PE; GFP-; GFP+; Tim3-APC; CD62L-PE/Cy7

B

Day 9 post-*Lm* RNAseq

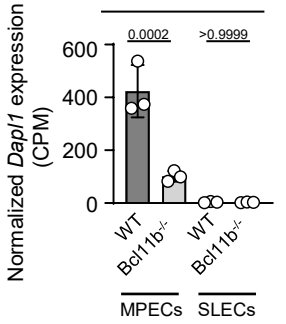

Supplementary figure 8

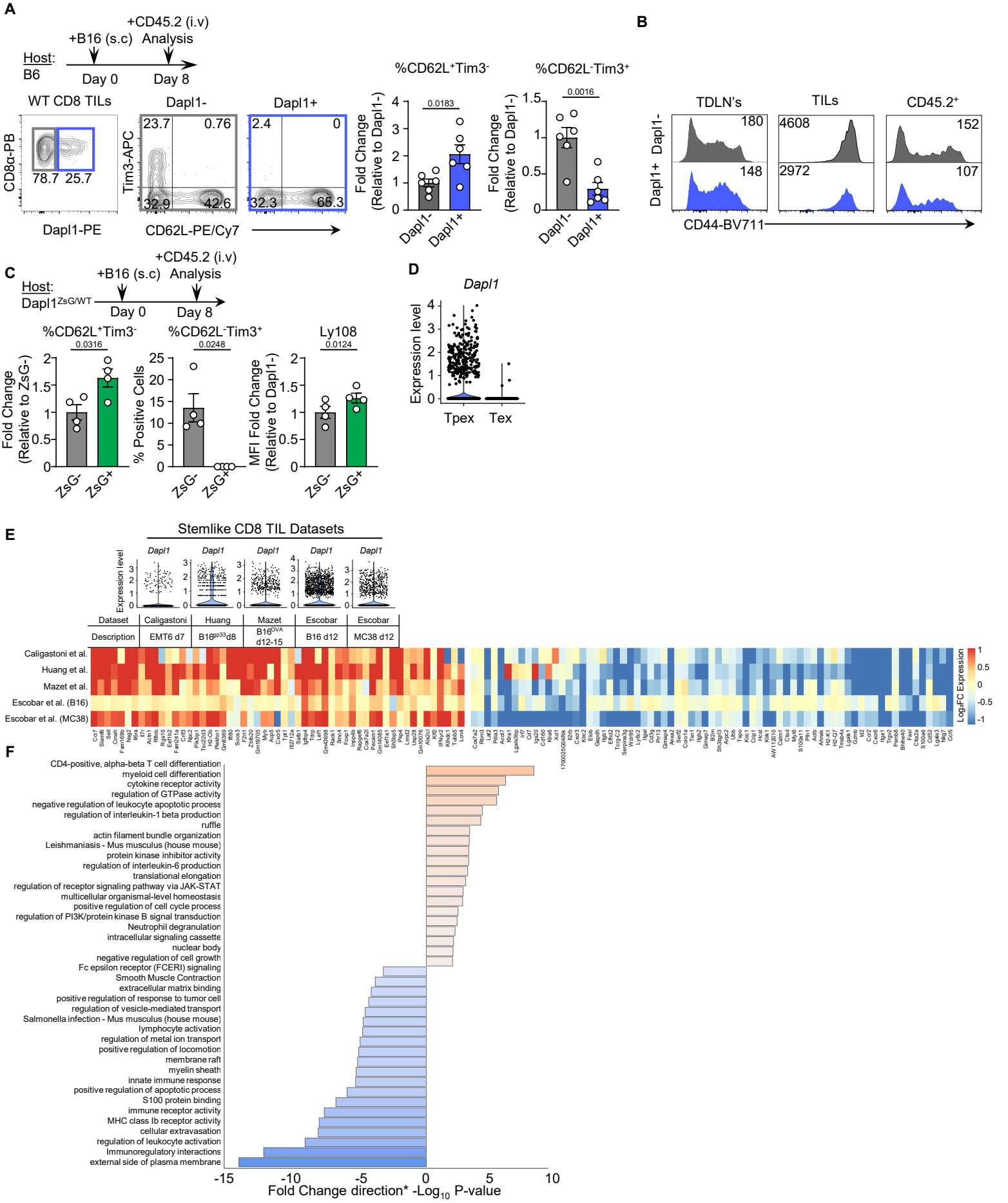

Supplementary figure 9

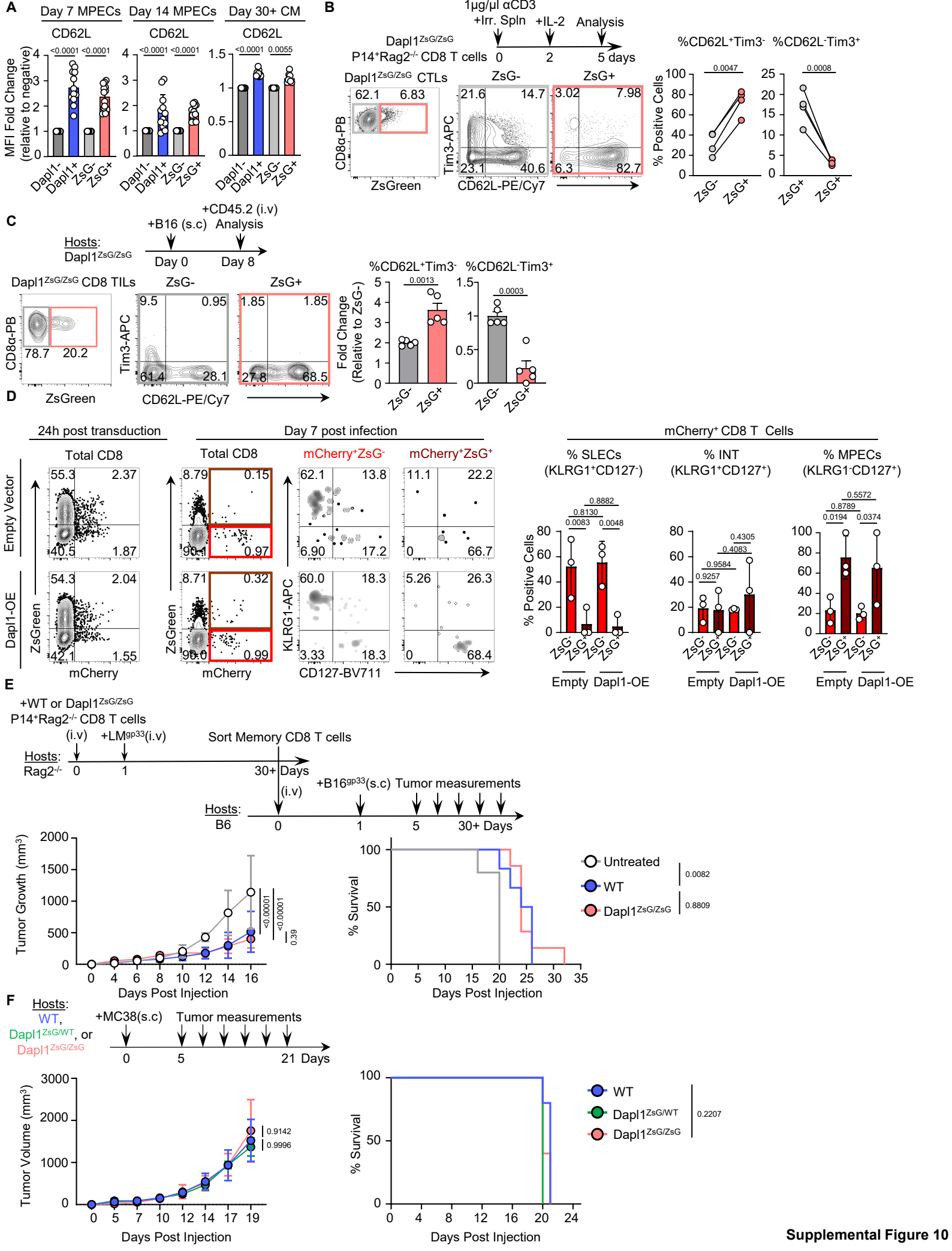

Supplemental Figure 10

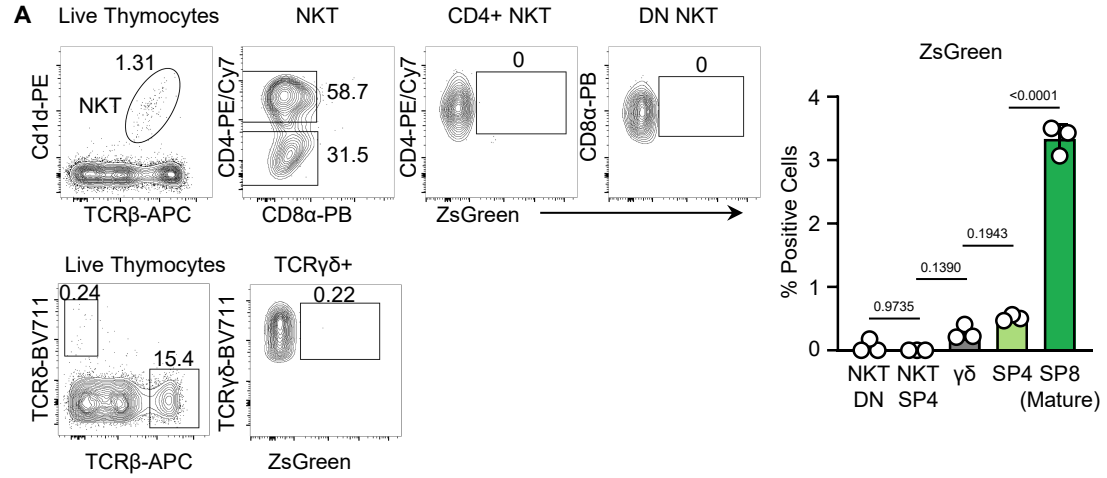
A
Live Thymocytes
NKT
CD4+ NKT
DN NKT
1.31
NKT
Cd1d-PE
TCRβ-APC
58.7
31.5
CD4-PE/Cy7
CD8α-PB
0
ZsGreen
CD8α-PB
Live Thymocytes
TCRγδ+
0.24
15.4
TCRδ-BV711
TCRβ-APC
0.22
TCRγδ-BV711
ZsGreen
ZsGreen
% Positive Cells
<0.0001
0.1943
0.1390
0.9735
NKT DN
NKT SP4
γδ
SP4
SP8 (Mature)

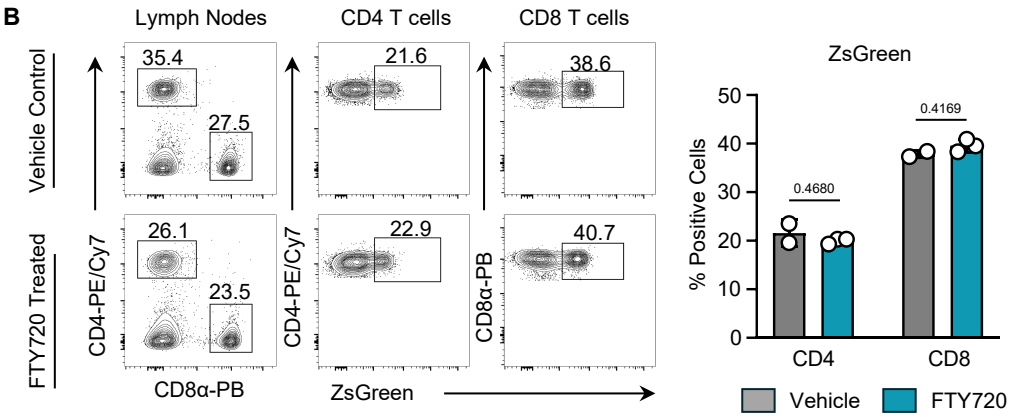
B
Lymph Nodes
CD4 T cells
CD8 T cells
Vehicle Control
FTY720 Treated
35.4
27.5
21.6
38.6
26.1
23.5
22.9
40.7
CD4-PE/Cy7
CD8α-PB
ZsGreen
ZsGreen
% Positive Cells
0.4680
0.4169
CD4
CD8
Vehicle
FTY720